

# Exactly solvable model for a velocity jump observed in crack propagation in viscoelastic sheets

Naoyuki Sakumichi<sup>1</sup> and Ko Okumura<sup>1,2</sup>

<sup>1</sup>Soft Matter Center, Ochanomizu University, Bunkyo-ku, Tokyo 112-8610, Japan

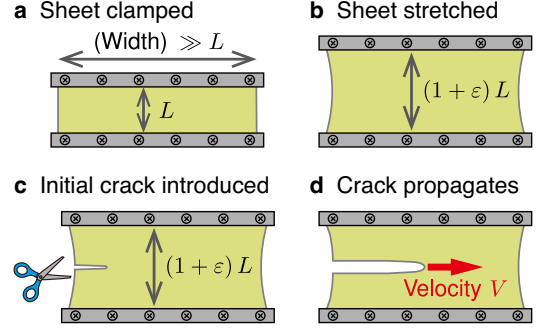
<sup>2</sup>Department of Physics, Ochanomizu University, Bunkyo-ku, Tokyo 112-8610, Japan

(Dated: June 17, 2019)

Needs to impart appropriate elasticity and high toughness to viscoelastic polymer materials are ubiquitous in industries such as concerning automobiles and medical devices, and such needs lead to novel ideas [1–5]. One of the major problems to overcome for toughening is catastrophic failure linked to a velocity jump, i.e., a sharp transition in the velocity of crack propagation occurred in a narrow range of the applied load [6–8]. However, its physical origin has remained an enigma despite previous studies over 35 years [9–12]. Here, we propose an exactly solvable model that exhibits the velocity jump based on the standard linear rubber rheology. With the exact solution, we elucidate the physical origin of the velocity jump: it emerges from a dynamical glass transition near ahead of the propagating crack tip. We further quantify the velocity jump together with slow and fast modes of crack propagation, which would stimulate the development of tough polymer materials.

Polymer-based viscoelastic materials are generally characterized by two elastic moduli  $E_0$  and  $E_\infty$  corresponding to (soft) rubber-like and (hard) glassy states, respectively [13, 14]. From this standard picture, one can understand generic features of the dependence of fracture energy on the velocity of crack propagation [15, 16]: the fracture energy  $G$  (twice the energy required to create crack surface of unit area [17]) starts from a static value  $G_0$  and increases with the velocity  $V$  to the value  $\lambda G_0$  with the ratio  $\lambda \equiv E_\infty/E_0$  ( $\simeq 10^2$ – $10^3$ ) [18–20]. This is because strong dissipation occurs at places far from the crack tip, whereas  $G_0$  is well described by the cutting energy of chemical bonds and an effective cross-link distance [21].

To further investigate dynamic properties of  $G$  as a function of  $V$ , crack-propagation experiment performed under a fixed-grip (or pure-shear) condition possesses significant advantages. We illustrate this experiment in Fig. 1a-d: a long sheet of height  $L$  is subject to a fixed strain  $\varepsilon$  before and after the initiation of crack propagation, unlike other experiments based on peeling, tearing, cyclic loads, etc. [22, 23]. Advantages of the fixed-grip experiment are also stressed in Ref. [10], and here we emphasize the following two points. (i) A steady-state crack propagation is realized with no work done by the external force, which leads to the equality  $G = wL$  with the initially applied elastic energy density  $w \equiv \int_0^\varepsilon \sigma(\varepsilon)d\varepsilon$ , where



e Experimental data [Tsunoda *et al.* (2000).]

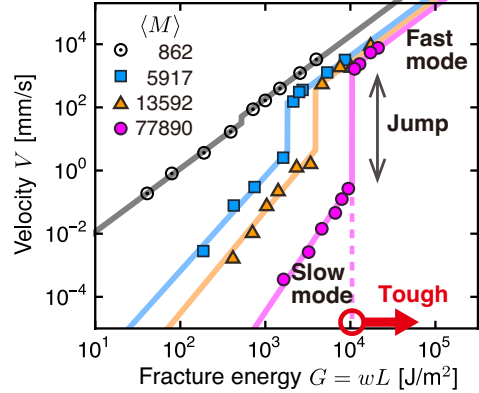


FIG. 1: **Velocity jump important for toughening, observed in the fixed-grip crack propagation.** a-d, Schematic illustrations of the fixed-grip crack propagation investigated in this study. To achieve a constant-velocity crack propagation, the following steps are performed. (a) The top and bottom edges of the sheet of height  $L$  are clamped. (b) The sheet is stretched to a fixed strain  $\varepsilon$ . (c) A small crack is introduced to initiate crack propagation. (d) After a short transient time, the crack propagates at a constant velocity  $V$  under the fixed strain  $\varepsilon$ . In the fixed-grip crack propagation, the fracture energy  $G$  and the strain energy release rate, which is simply expressed as  $wL$  under the fixed-grip condition, take the same value:  $G = wL$ . Here,  $w$  is the initially applied energy density. e, Typical experimental results,  $G$  vs.  $V$ , obtained from the fixed-grip crack propagation by using elastomers filled with carbon black particles (taken from Ref. [11]). With the increase in velocity, the slow-mode regime (corresponding to a straight line on the low-velocity side) is terminated by an abrupt velocity jump, after which follows the fast-mode regime (corresponding to a straight line on the high-velocity side). Here,  $\langle M \rangle$  represent the average molar mass between nearest cross-links. In this series of experiments, the systematic increase in the cross-link distance leads to the increase in the transition energy.

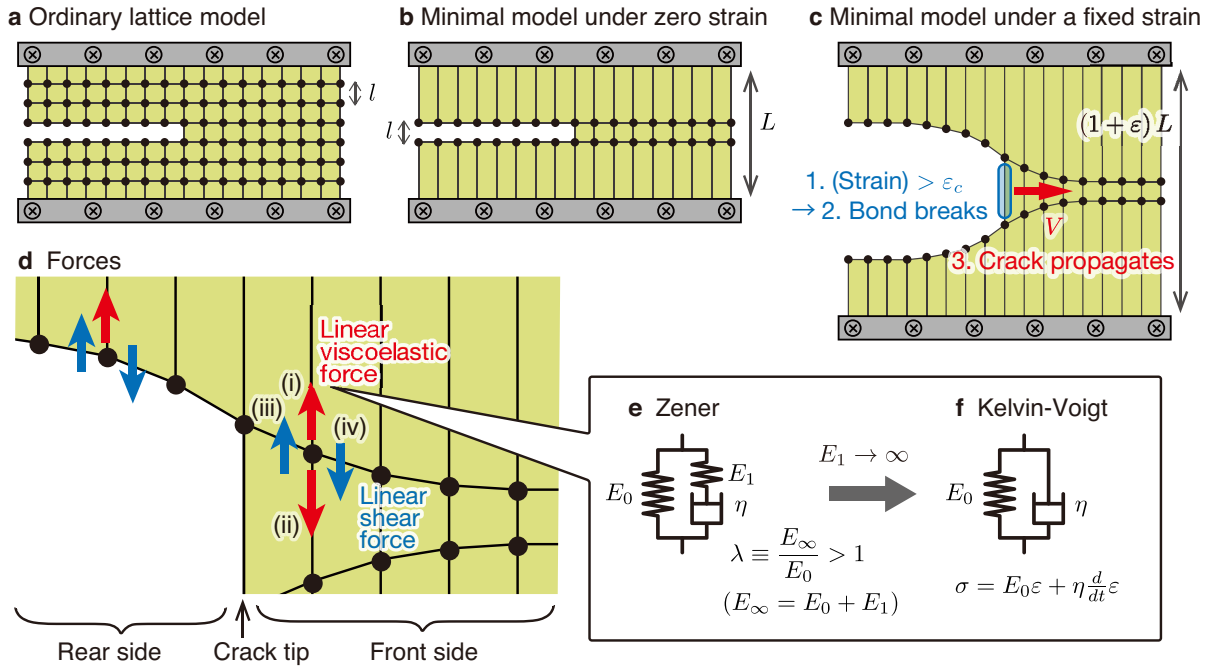


FIG. 2: **Minimal model for the fixed-grip crack propagation.** **a**, Two-dimensional square-lattice model of a sheet with a line crack. Here,  $l$  is the lattice spacing. Each lattice point interacts with the nearest-neighbor points. We introduce a line crack by cutting bonds, i.e., we set the interactions of the corresponding bonds to zero. **b**, Minimal model obtained by coarse-graining the lattice in (a). We decimate all the lattice points except for the points on the two horizontal lines on which the two surfaces of the line crack are positioned, where  $L$  is the height of the sheet under zero strain. **c**, Mechanism of the crack propagation. When the spring at the crack tip (encircled by a blue ellipse) is stretched to the critical strain  $\varepsilon_c$ , the bond at the tip breaks, and, after a certain time, the next bond at the tip is stretched to  $\varepsilon_c$ . This cycle continues during the crack propagation. **d**, Forces acting on a lattice point. On each point in (c) located at the front side of the crack tip, four forces act: (i) one from the top boundary, (ii) one from the point below, and (iii, iv) the remaining two reflecting shear and acting from the left and right nearest-neighbor points. For each point located at the rear side, one force from the point below is missing. **e**, Zener element. This element is a parallel connection of two components: a spring (the elastic modulus  $E_0$ ) and a serial connection (a Maxwell element) of another spring (the modulus  $E_1$ ) and a dashpot (the viscosity  $\eta$ ). **f**, Kelvin-Voigt element obtained from a Zener element in the large  $E_1$  limit, in which  $\lambda \equiv E_\infty/E_0 \rightarrow \infty$ .

$\sigma$  is the stress [8, 22, 24]. (ii) As shown in Fig. 1e, the  $G$ - $V$  plots exhibit an intriguing structure: the velocity  $V$  jumps at a critical value  $G = G_c$ , causing a transition from the slow ( $V \lesssim 1$  mm/s) to fast ( $V \gtrsim 10^3$  mm/s) mode [6–8]. This  $G$ - $V$  structure reveals that toughness is achieved by increasing the critical value  $G_c$  because such an increase reduces the risk of a velocity jump, which can trigger catastrophic failure.

Theoretical understanding of the velocity jump has been very limited, although it is important for toughening materials. Previous theories based on linear fracture mechanics [17] and linear viscoelasticity [13] are unable to reproduce the velocity jump [9–11]. Although there is a theory that reproduces the jump [12], the theory predicts an extremely high-temperature region near the crack tip whereas only a slight temperature-increase was experimentally observed [25].

In this Letter, we propose a minimal model that exhibits the velocity jump observed in the fixed-grip crack propagation, incorporating the standard linear rubber rheology described by the two elastic moduli  $E_0$  and  $E_\infty$ .

This is performed with a spirit similar to the ones with which one of the authors constructed simple and useful models for biological composites [26–28]. From the proposed model, we obtain successfully an exact analytical relation between the initially applied energy density  $w$  and the crack-propagation velocity  $V$ . As a result, we find simple expressions characterizing the transition point. These expressions provide guiding principles to reduce the risk of the jump, which can trigger catastrophic failure. Besides, we elucidate the physical mechanism that leads to the jump, indicating a direct link to a glass transition at the crack tip, and we show that the jump could be universally observed in a broad class of materials.

Specifically, we construct the minimal model as follows. Starting from the two-dimensional square-lattice model (Fig. 2a), often used to simulate the structure and dynamics of sheet materials, we derive a simplified model illustrated in Fig. 2b by decimating most of the lattice points. As illustrated in Fig. 2c, the survivors (lattice points) represent the minimum number of variables es-

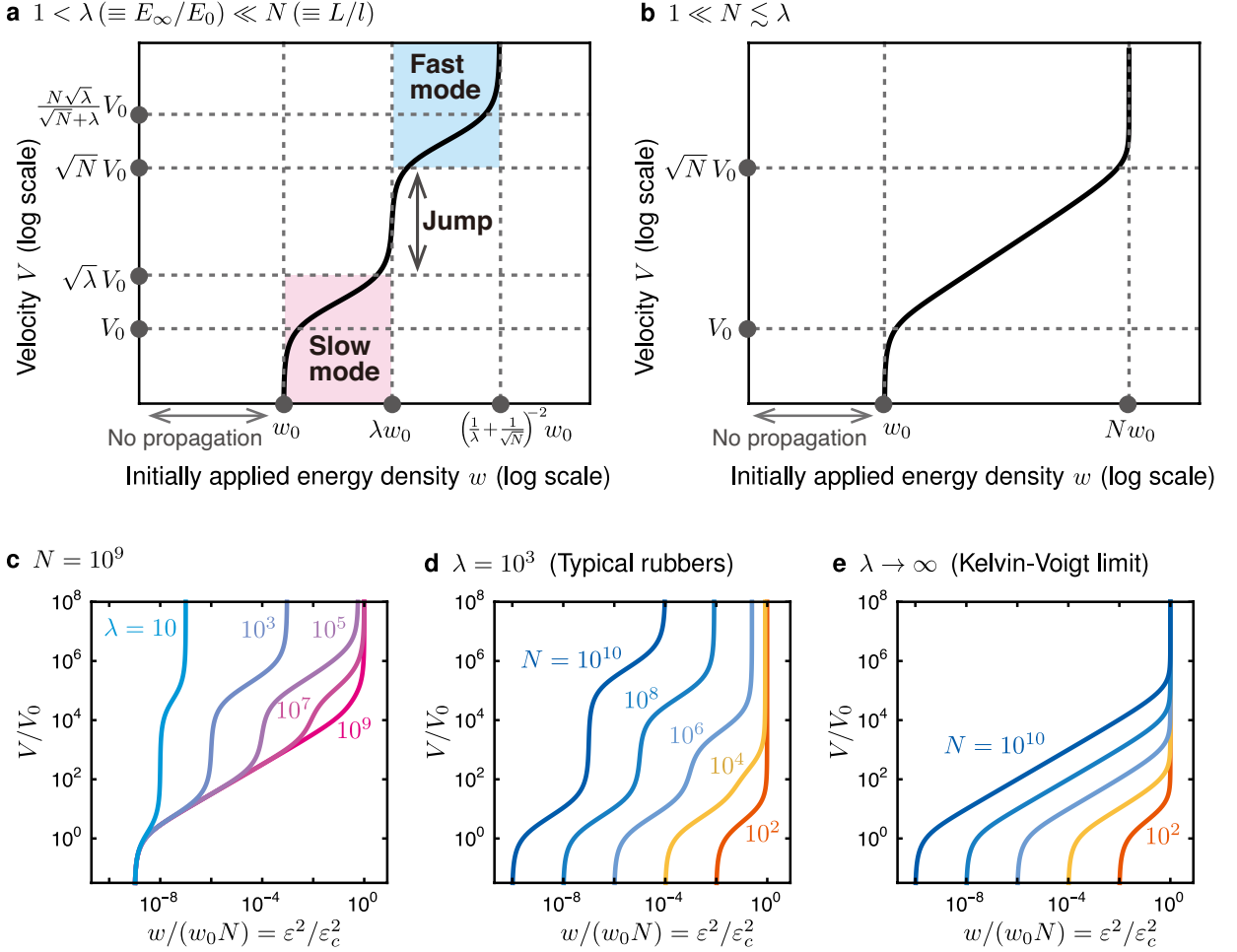


FIG. 3: **Reproduced velocity jump and simple characterization of the  $w$ - $V$  curve.** **a-b**, Two representative plots of the crack propagation velocity  $V$  as a function of the initially applied energy density  $w$ . The cases (a) with and (b) without velocity jump are obtained for  $1 < \lambda \ll N$  and  $1 \ll N \lesssim \lambda$ , respectively. Four characteristic velocity-scales and three energy-scales are indicated in (a), which are important for toughening. **c-e**,  $V/V_0$  vs.  $w/(w_0N) = \varepsilon^2/\varepsilon_c^2$ , obtained from Eq. (1) on a log-log scale. The normalization factors for velocity and energy are  $V_0 \simeq lE_0/\eta$  and  $w_0 \equiv E_0\varepsilon_c^2/(2L)$ , respectively. The cases with velocity jump are demonstrated for various  $\lambda$  with a fixed  $N$  in (c) and for various  $N$  with a fixed  $\lambda$  in (d). The Kelvin-Voigt limit,  $\lambda \rightarrow \infty$ , is shown for various  $N$  in (e) as an example of the case without velocity jump.

sential for the description of crack propagation. To realize the propagation of a crack in the  $x$ -direction, each bond is assumed to break if the local strain at the crack tip is larger than the critical strain  $\varepsilon_c$ .

We explain the forces acting on each remaining lattice point in Fig. 2d. For simplicity, we assume that Poisson's ratio is zero. Thus, the forces always orient towards the  $y$ -direction and each point can move only in the  $y$ -direction (See Supplementary Section 1 for the details). The shear force is linear elastic, and the normal force is described by the Zener element in Fig. 2e characterized by two elastic moduli ( $E_0$  and  $E_\infty$ ) and viscous dissipation ( $\eta$ ), as in de Gennes' trumpet model [18–20]. As illustrated in Fig. 4a-b below, when slowly stretched, a Zener element behaves as a (rubber-like) soft solid because the dashpot moves freely without any friction: the elastic modulus is small and approximately given by  $E_0$ .

When rapidly stretched, a Zener element behaves as a (glassy) hard solid because the dashpot does not have enough time to move: the elastic modulus is large and approximately given by  $E_\infty$ . Note that a Zener element reduces to a Kelvin-Voigt element when  $\lambda \equiv E_\infty/E_0 \rightarrow \infty$  (Fig. 2f).

The minimal model allows us to derive the exact analytical relation between  $w = G/L$  and  $V$ , in a continuum limit in the  $x$ -direction. The result is summarized below (See Methods for the derivations). Since the present model is initially (before the crack propagates) at rest with a fixed  $\varepsilon$  without shear, it behaves as a linear elastic material governed by  $\sigma = E_0\varepsilon$  and the initially applied energy density is given by  $w = E_0\varepsilon^2/2$ . Let  $N \equiv L/l$  be the dimensionless parameter of the length scale in the  $y$ -direction. For  $\varepsilon \leq \varepsilon_c/\sqrt{N}$  the crack does not propagate ( $V = 0$ ) and for  $\varepsilon \geq \varepsilon_c\lambda/(\sqrt{N} + \lambda - 1)$  any

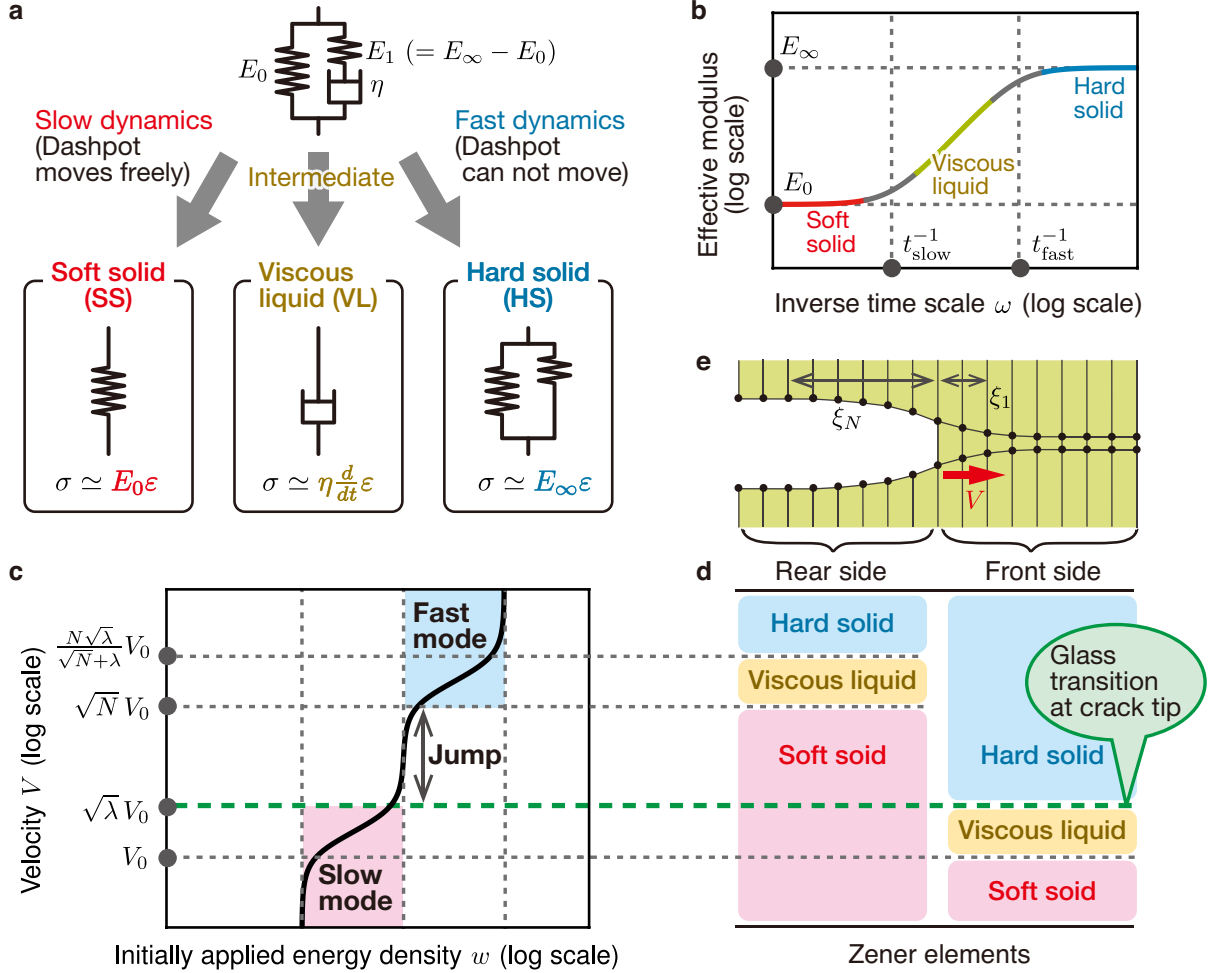


FIG. 4: **Whole physical pictures on the crack propagation: glass-transition induced velocity jump.** **a**, Three dynamic regimes of a Zener element: soft-solid, viscous-liquid, and hard-solid regimes. This time dependence emerges from the stress-strain relation of a Zener element:  $(1 + t_{fast} \frac{d}{dt})\sigma(t) = (1 + t_{slow} \frac{d}{dt})E_0\varepsilon(t)$  with  $t_{fast} \equiv \eta/E_1 \simeq \eta/E_\infty$  and  $t_{slow} \equiv \eta/E_0 + \eta/E_1 \simeq \eta/E_0$ . In the soft-solid and hard-solid regimes the dynamics are governed by the springs characterized by  $E_0$  and  $E_\infty$ , respectively, whereas in the viscous-liquid regime the dynamics is governed by the dashpot characterized by  $\eta$ . **b**, Effective elastic modulus as a function of inverse time scale  $\omega$  in a Zener element. Here, the effective elastic modulus is estimated as  $\frac{1+\omega t_{slow}}{1+\omega t_{fast}} E_0$  at the level of scaling laws ( $d/dt \sim \omega$ ). **c-e**, Physical pictures for the crack propagation revealed by the present exact solution for  $\lambda \ll N$ . The four velocity scales in plot (c) correspond to crossover points among Zener elements in the rear and front sides of the crack tip shown in (d). The illustration (e) implies the definition of the healing lengths  $\xi_1$  and  $\xi_N$ .

constant-velocity solutions do not exist: the crack propagates only in the range  $\varepsilon_c/\sqrt{N} < \varepsilon < \varepsilon_c\lambda/(\sqrt{N} + \lambda - 1)$ , or equivalently, in the range  $w_0 < w < w_\infty$ . Here,  $w_0$  ( $\equiv E_0\varepsilon_c^2/(2N)$ ) and  $w_\infty$  are the minimum and maximum values of  $w$  for the propagation, respectively. In this range, the relation between  $w = G/L$  and  $V$  is given by

$$\frac{w}{w_0} = N \left[ \frac{\frac{1}{\lambda-1} \left( \frac{N}{\xi_1 \xi_N} + \lambda \right) \frac{V}{V_0} + \xi_1 + \xi_N}{\frac{1}{\lambda-1} \left( N + \frac{N}{\xi_1 \xi_N} + \lambda - 1 \right) \frac{V}{V_0} + N\xi_1 + \xi_N} \right]^2, \quad (1)$$

with  $V_0 \equiv \frac{l}{\eta} \sqrt{\frac{1}{2} \left( 1 - \frac{1}{N} \right) E_0 \mu}$  where  $\mu$  is an effective shear

modulus. In the practical case with  $l \ll L$  in which  $\mu$  scales as  $E_0$ , the velocity  $V_0$  scales as  $l/t_0$  with  $t_0 \equiv \eta/E_0$  where  $l$  is the smallest length scale in the present problem. Here,  $\xi_N$  is the positive real solution of the following cubic equation for  $\xi$ :

$$\xi^3 + \frac{\lambda V}{(\lambda-1)V_0} \xi^2 - N\xi - \frac{NV}{(\lambda-1)V_0} = 0, \quad (2)$$

which has a unique positive real solution as guaranteed by Supplementary Lemma 1. The explicit form of  $\xi_N$  is given by Cardano's formula for the solution of a cubic equation. We obtain  $\xi_1$  by substituting  $N = 1$  to  $\xi_N$ .

As illustrated in Fig. 3a, Eq. (1) guarantees the existence of the velocity jump for  $\lambda \ll N$ . The existence

condition  $\lambda \ll N \equiv L/l$  is derived in Supplementary Theorem 3 and is well satisfied in typical viscoelastic elastomers for regular specimen sizes ( $\lambda \simeq 10^3$ ,  $L \simeq 10$  cm, and  $l \simeq 10$  nm). Since viscoelastic models are frequently used to describe viscoplastic materials such as resins under certain constraints [17], the present model could be relevant to a broad class of materials beyond viscoelastic materials: the velocity jump is expected to be a universal phenomenon even in viscoplastic materials. Note that the present model fails to reproduce the velocity jump for  $\lambda \gtrsim N$  (including the Kelvin-Voigt limit,  $\lambda \rightarrow \infty$ ) as illustrated in Fig. 3b. Figure 3c-e demonstrates how Eq. (1) depends on  $\lambda$  and  $N$ .

The exact relation in Eq. (1) leads to simple expressions for the four points characterizing the  $w$ - $V$  curve given in Fig. 3a, such as  $(w_0, V_0)$  and  $(\lambda w_0, \sqrt{\lambda}V_0)$ . These simple expressions are useful for controlling crack propagation in developing tough materials. In particular, the point  $(\lambda w_0, \sqrt{\lambda}V_0)$  shows that the velocity jump occurs at  $w = w_c (= G_c/L)$ , where

$$w_c \equiv \lambda w_0 = \frac{lE_\infty \varepsilon_c^2}{2L}. \quad (3)$$

Equation (3) gives the following guiding principles to develop tough polymer materials (i.e., to reduce the risk of a velocity jump, which can trigger catastrophic failure): keeping the principal elasticity  $E_0$ , we can increase the transition energy density  $w_c$  by increasing (i) the modulus  $E_\infty$  in the glassy state and/or (ii) the lattice spacing  $l$ . Here,  $l$  can be regarded as a characteristic length scale below which the continuum description is no longer valid:  $l$  is the largest length scale among the cross-link distance, the size of filler particles, the filler-particle distance, and the length scale of possible inhomogeneous structures in the sample.

The transition energy density  $w_c$  given in Eq. (3) is consistent with empirical knowledge in polymer science. For instance, Fig. 1e experimentally shows that the transition energy  $G_c = w_c L$  increases as the cross-link distance (i.e., the parameter  $l$ ) increases [7]. This feature is consistent with Eq. (3) because  $E_\infty$  and  $\varepsilon_c$  are approximately constant even for different  $\langle M \rangle$  in Fig. 1e (see, e.g., Ref. [8]).

We can elucidate the physical origin of the velocity jump emerging from Eq. (1), as illustrated in Fig. 4. A Zener element exhibits a crossover among three regimes depending on the time scale of the dynamics (Fig. 4a-b): soft solid (SS), viscous liquid (VL), and hard solid (HS). Corresponding to this, the equations of motion for the lattice points exhibit crossovers among three regimes (SS, VL, and HS), depending on the velocity  $V$  and on whether the lattice point is located on the front or rear side (Fig. 4c-e). Figure 4d illustrates the dynamic behaviors of Zener elements on the front and rear sides changing with the velocity  $V$ , indicating the physical pictures for the slow and fast modes and the velocity jump: (i) the slow ( $V < \sqrt{\lambda}V_0$ ) and fast ( $\sqrt{N}V_0 < V$ ) modes are characterized by the viscous dissipation on the

front and rear sides, respectively; (ii) the velocity jump ( $\sqrt{\lambda}V_0 < V < \sqrt{N}V_0$ ) starts at the VL-HS crossover on the front side and ends at the SS-VL crossover on the rear side.

If we regard the VL-HS crossover as a dynamic glass transition, the onset of the velocity jump at  $V = \sqrt{\lambda}V_0$  (the green dashed line in Fig. 4d) can be interpreted as the glass transition at the crack tip on the front side. Note that the glass transition occurs at a lower velocity on the front side than on the rear side, because the material is more stretched on the front side. This fact implies that glass transitions are easy to occur in the crack-propagation experiment, and thus, we expect that even materials such as gels, in which glass transitions are difficult to occur, could exhibit the velocity jump.

The present results would be useful both from practical and fundamental viewpoints. (i) Conventionally the development of new materials tends to be achieved by trials and errors; however, the expressions for the points characterizing the curve in Fig. 3a are simple enough to remove such trials and errors, and pave the way for a more efficient development of tough polymer materials. (ii) We point out an analogy to conventional phase transitions. The stress and strain distributions naturally lead to the healing lengths  $\xi_N$  and  $\xi_1$  (see Fig. 4e); these lengths play roles of order parameters in the context of conventional phase transitions such as superconductors and Bose-Einstein condensations [29] (see Supplementary Fig. S4). (iii) Equation (5) in Methods for  $\lambda \rightarrow \infty$  belongs to the class of reaction-diffusion equation [30], and the counterpart for arbitrary  $\lambda$  forms a generalized class. The present generalization could enrich physical scenarios in reaction-diffusion systems in different disciplines, e.g., pattern formation in chemical reaction systems and morphogenesis in biology.

## Methods

### Derivation of the relation between $w$ and $V$ .

To explain how to derive the exact relationship between  $w$  and  $V$  given in Eq. (1), we first consider a more simplified model consisting of Kelvin-Voigt elements illustrated in Fig. 2f. We obtain a Kelvin-Voigt element from the present model in the limit  $\lambda \rightarrow \infty$ . Although this simpler model does not reproduce the velocity jump (see Fig. 3b and 3e), it is useful to understand the mathematical structure of the present model. For simplicity, we assume that the sheet is symmetric about the  $x$ -axis and consider only the lattice points on the upper side (see Fig. 2c). Let  $u_i$  be the  $y$ -coordinate of the  $i$ -th point. The dynamics of lattice points located on the front side (right-hand side of the crack tip, see Fig. 2d) is governed by the following equation of motion in the  $y$ -direction:

$$m \frac{\partial^2 u_i}{\partial t^2} = -ku_i - \zeta \frac{\partial u_i}{\partial t} + K(u_i - u_{i+1} + u_i - u_{i-1}). \quad (4)$$

Here,  $ku_i$  and  $\zeta \partial u_i / \partial t$  are the elastic and viscous forces (acting from the top boundary and the point below), and  $K(u_i - u_{i+1} + u_i - u_{i-1})$  is the shear force (acting from the left and right nearest-neighbor points). Taking a continuum limit in the  $x$ -direction with replacing  $u_i - u_{i+1} + u_i - u_{i-1}$  by  $l^2 \partial^2 u(x, t) / \partial x^2$  and assuming that we can neglect the inertial term  $m \partial^2 u_i / \partial t^2$  (the overdamped limit), we rewrite Eq. (4) as

$$0 = -ku(x, t) - \zeta \frac{\partial}{\partial t} u(x, t) + l^2 K \frac{\partial^2}{\partial x^2} u(x, t). \quad (5)$$

To seek a solution corresponding to a constant-velocity crack propagation, we substitute the form  $u(x, t) = f(x - Vt)$  into Eq. (5) to obtain a linear ordinary differential equation (ODE):

$$0 = -kf(x) + V\zeta f'(x) + l^2 K f''(x). \quad (6)$$

The equation of motion corresponding to Eq. (6) for the lattice points located on the rear side (left-hand side of the crack tip, see Fig. 2d) is given by the same equation but with the values of the spring constant  $k$  and viscous damping coefficient  $\zeta$  being different because one of the four forces is missing ( $k$  and  $\zeta$  are described by  $E_0$ ,  $\eta$ ,  $l$  and  $L$ ). We can solve the front and rear equations with appropriate boundary conditions at  $x = \pm\infty$  and matching condition of the front and rear solutions at the crack tip (See Supplementary Section 2 for the details).

As a result, we find that crack propagates only in the range  $1/\sqrt{N} < \tilde{\varepsilon} < 1$  or equivalently  $w_0 < w < w_0 N$ , and the velocity is exactly given by

$$\frac{V}{V_0} = \frac{N\tilde{\varepsilon}^2 - 1}{\sqrt{N\tilde{\varepsilon}(1 - \tilde{\varepsilon})(N\tilde{\varepsilon} - 1)}}, \quad (7)$$

with  $\tilde{\varepsilon} \equiv \varepsilon/\varepsilon_c = \sqrt{w/(w_0 N)}$ . Equation (7) for the model consisting of Kelvin-Voigt elements is the counterpart of Eq. (1) for the model consisting of Zener elements. In fact, by taking the limit  $\lambda \rightarrow \infty$  in Eq. (1), we have Eq. (7), which does not reproduce the velocity jump (Fig. 3e), unlike Eq. (1).

We next briefly describe how to generalize the above procedure to the model consisting of Zener elements illustrated in Fig 2e. The counterpart of Eq. (5) is expressed as coupled equations of motion:  $0 = -ku - \zeta \frac{\partial}{\partial t} u_2 + l^2 K \frac{\partial^2}{\partial x^2} u$  and  $E_1 u_1 = \eta \frac{\partial}{\partial t} u_2$ , with the elongation of dashpot  $u_2$  and the total elongation  $u = u_1 + u_2$ . By noting the relation  $u = \frac{\eta}{E_1} \frac{\partial}{\partial t} u_2 + u_2$ , the equation of motion can be written only in terms of  $u_2$  by removing the variables  $u$  and  $u_1$ . Introducing the form  $u_2(x, t) = f_2(x - Vt)$  as before, we obtain a third-order linear ODE for  $f_2$ , which can be solved under the boundary conditions including the matching condition of the front and rear solutions. As a result, we obtain Eq. (1) together with Eq. (2), which is a characteristic equation of the third-order linear ODE for  $f_2$ . We explain the details of the derivation in Supplementary Section 3.

## Acknowledgments

The authors thank Katsuhiko Tsunoda for providing us with experimental data that we reproduced in Fig. 1e. The authors thank Katsuhiko Tsunoda, Yoshihiko Morishita, Kohzo Ito, Kenji Urayama, Hiroya Kodama, Atsushi Kubo, Yoshitaka Umeno, Jian Ping Gong, Atsushi Takahara, and Yuko Aoyanagi for fruitful discussions. N. S. thanks Hiroki Fukagawa, Tetsuo Hattusuda, Atsushi Ikeda, Akira Shimizu, and Hal Tasaki for useful comments, and is supported by JSPS KAKENHI Grant Number 15K17725. This research was partly supported by Grant-in-Aid for Scientific Research (A) (No. 24244066) of JSPS, Japan, and by ImPACT Program of Council for Science, Technology and Innovation (Cabinet Office, Government of Japan).

[1] Gong, J. P., Katsuyama, Y., Kurokawa, T. & Osada, Y. Double-network hydrogels with extremely high mechanical strength. *Ad. Mater.* **15**, 1155–1158 (2003).  
 [2] Sun, T. L. *et al.* Physical hydrogels composed of polyampholytes demonstrate high toughness and viscoelasticity. *Nature Mater.* **12**, 932–937 (2013).

[3] Ducrot, E., Chen, Y., Bulters, M., Sijbesma, R. P. & Creton, C. Toughening elastomers with sacrificial bonds and watching them break. *Science* **344**, 186–189 (2014).  
 [4] Okumura, Y. & Ito, K. The polyrotaxane gel: A topological gel by figure-of-eight cross-links. *Ad. Mater.* **13**, 485–487 (2001).

- [5] Sakai, T. *et al.* Design and fabrication of a high-strength hydrogel with ideally homogeneous network structure from tetrahedron-like macromonomers. *Macromolecules* **41**, 5379–5384 (2008).
- [6] Kadir, A. & Thomas, A. G. Tear behavior of rubbers over a wide range of rates. *Rubber Chem. Tech.* **54**, 15–23 (1981).
- [7] Tsunoda, K., Busfield, J. J. C., Davies, C. K. L. & Thomas, A. G. Effect of materials variables on the tear behaviour of a non-crystallising elastomer. *J. Mater. Sci.* **35**, 5187–5198 (2000).
- [8] Morishita, Y., Tsunoda, K. & Urayama, K. Velocity transition in the crack growth dynamics of filled elastomers: Contributions of nonlinear viscoelasticity. *Phys. Rev. E* **93**, 043001 (2016).
- [9] Greenwood, J. A. & Johnson, K. L. The mechanics of adhesion of viscoelastic solids. *Phil. Mag. A* **43**, 697–711 (1981).
- [10] Barber, M., Donley, J. & Langer, J. S. Steady-state propagation of a crack in a viscoelastic strip. *Phys. Rev. A* **40**, 366 (1989).
- [11] Persson, B. N. J. & Brener, E. A. Crack propagation in viscoelastic solids. *Phys. Rev. E* **71**, 036123 (2005).
- [12] Carbone, G. & Persson, B. N. J. Hot cracks in rubber: origin of the giant toughness of rubberlike materials. *Phys. Rev. Lett.* **95**, 114301 (2005).
- [13] Ferry, J. D. *Viscoelastic properties of polymers* (John Wiley & Sons, New York, 1980).
- [14] Doi, M. & Edwards, S. F. *The theory of polymer dynamics* (Oxford Univ. Press, Oxford, 1988).
- [15] Gent, A. N. Adhesion and strength of viscoelastic solids. Is there a relationship between adhesion and bulk properties? *Langmuir* **12**, 4492–4496 (1996).
- [16] Kashima, Y. & Okumura, K. Fracture of soft foam solids: Interplay of visco- and plasto-elasticity. *ACS Macro Lett.* **3**, 419–422 (2014).
- [17] Anderson, T. L. *Fracture Mechanics: Fundamentals and Applications* 3rd ed. (CRC Press, Boca Raton, Florida, 2005).
- [18] de Gennes, P. G. Soft adhesives. *Langmuir* **12**, 4497–4500 (1996).
- [19] de Gennes, P. G. *Soft interfaces: the 1994 Dirac memorial lecture* (Cambridge Univ. Press, Cambridge, 2005).
- [20] Saulnier, F., Ondarcuhu, T., Aradian, A. & Raphaël, E. Adhesion between a viscoelastic material and a solid surface. *Macromolecules* **37**, 1067–1075 (2004).
- [21] Lake, G. L. & Thomas, A. G. The strength of highly elastic materials *Proc. R. Soc. A* **300**, 108–119 (1967).
- [22] Lake, G. L. Fracture mechanics and its application to failure in rubber articles. *Rubber Chem. Tech.* **76**, 567–591 (2003).
- [23] Busfield, J. J. C., Tsunoda, K., Davies, C. K. L. & Thomas, A. G. Contributions of time dependent and cyclic crack growth to the crack growth behavior of non strain-crystallizing elastomers. *Rubber Chem. Tech.* **75**, 643–656 (2002).
- [24] Rivlin, R. S. & Thomas, A. G. Rupture of rubber. I. Characteristic energy for tearing. *J. Polym. Sci.* **10**, 291–318 (1953).
- [25] D’Amico, F. D., Carbone, G., Foglia, M. M. & Galietti, U. Moving cracks in viscoelastic materials: Temperature and energy-release-rate measurements. *Eng. Frac. Mech.* **98**, 315–325 (2013).
- [26] Okumura, K. & de Gennes, P. G. Why is nacre strong? elastic theory and fracture mechanics for biocomposites with stratified structures. *Eur. Phys. J. E* **4**, 121–127 (2001).
- [27] Aoyanagi, Y. & Okumura, K. Simple model for the mechanics of spider webs. *Phys. Rev. Lett.* **104**, 038102 (2010).
- [28] Okumura, K. Strength and toughness of biocomposites consisting of soft and hard elements: A few fundamental models. *MRS Bulletin* **40**, 333–339 (2015).
- [29] Leggett, A. J. *Quantum Liquids: Bose condensation and Cooper pairing in condensed-matter systems* (Oxford Univ. Press, Oxford, 2006).
- [30] Smoller, J. *Shock Waves and Reaction Diffusion Equations* (Springer-Verlag, New York-Berlin, 1994).

## Supplementary Information: Exactly solvable model for a velocity jump observed in crack propagation in viscoelastic sheets

In this note, we explain the details of the formulation of the model and the derivation of the analytical solutions given in the main text. This note is organized as follows. In Sec. I, we describe a lattice model for the fixed-grip crack propagation in viscoelastic sheets with incorporating Kelvin-Voigt elements for the interaction between the lattice points. In Sec. II, we construct a model for which an analytical solution is available for a constant-velocity crack propagation, by simplifying the ordinary lattice model introduced in Sec. I. For the model consisting of Kelvin-Voigt elements, we derive an analytical expression for the crack-propagation velocity as a function of the initially applied energy density and show that the model does not exhibit the velocity jump. In Sec. III, we replace the Kelvin-Voigt interaction with the Zener interaction in the model. For the model consisting of Zener elements, we derive an analytical expression for the crack-propagation velocity as a function of the initially applied energy density and reveal that the model exhibits the velocity jump. In Sec. IV, from the analytical solution, we derive the existence condition of the velocity jump, together with simple relations useful for controlling crack propagation in developing tough materials.

### I. LATTICE MODEL CONSISTING OF KELVIN-VOIGT ELEMENTS

We construct a lattice model for crack propagation in a viscoelastic sheet, which satisfies the following conditions:

- The viscoelastic sheet is always on the  $x$ - $y$  plane. Under zero strain, the height (in the  $y$ -direction) and thickness (in the  $z$ -direction) of the sheet are  $L$  and  $h$ , respectively, whereas the width (in the  $x$ -direction) is much larger than  $L$ .
- The fixed strain  $\varepsilon$  ( $\equiv \Delta L/L \geq 0$ ) is applied in the  $y$ -direction.
- A line crack propagates in the positive  $x$ -direction.

We consider a two-dimensional model on an  $N_1 \times N_2$  rectangular lattice where  $N_1$  is (countably) infinite and  $N_2$  is even. The lattice points are labeled by the index  $\mathbf{n} = (n_1, n_2)$  where  $n_1 \in \mathbb{Z} \equiv \{\dots, -1, 0, 1, \dots\}$  and  $n_2 \in \{1, 2, \dots, N_2\}$ . At  $\varepsilon = 0$ , the lattice constant in the  $x$ - and  $y$ -direction are  $a$  and  $b$ , respectively. In other words, under zero strain, the height and width of the sheet are  $aN_1 (= \infty)$  and  $bN_2 (= L)$ , respectively. The position of the lattice point labeled by the index  $\mathbf{n}$  is given by  $\mathbf{r}_0(\mathbf{n}) = (an_1, bn_2 - L/2)$ . When the top and bottom edges of the sheet are clamped and stretched in the  $y$ -direction ( $\varepsilon > 0$ ), we set the coordinate of the points on the edges to  $\mathbf{r}_\varepsilon(n_1, 1) = (an_1, -L(1 + \varepsilon)/2)$  and  $\mathbf{r}_\varepsilon(n_1, N_2) = (an_1, L(1 + \varepsilon)/2)$ . The displacement of the lattice point  $\mathbf{n}$  is given by  $\mathbf{r}_\varepsilon(\mathbf{n}) - \mathbf{r}_0(\mathbf{n}) \equiv \mathbf{u}(\mathbf{n}) = (u_1(\mathbf{n}), u_2(\mathbf{n}))$ .

In the model, every lattice point interacts with the nearest neighbor points (at most four points) by a minimal coupling. The normal and shear stresses  $F_{\text{normal}}$  and  $F_{\text{shear}}$  are given as  $F_{\text{normal}}/(ah) = E\Delta b/b$  and  $F_{\text{shear}}/(bh) = G\Delta b/a$ , respectively, for the deformation characterized by  $\Delta b$  (See, Fig. S1 for the case in which the unit cell deforms in the  $y$ -direction). Here, we have introduced Young's modulus  $E$  and the shear modulus  $G$ . The elastic energy of the sheet with the minimal coupling is then given by

$$U[u_\mu(\mathbf{n})] = h \sum_{n_1=-\infty}^{\infty} \sum_{n_2=1}^{N_2} \sum_{\mu=1}^2 \sum_{\nu=1}^2 \frac{1}{2} C_{\mu\nu} [u_\mu(\mathbf{n} + \hat{\nu}) - u_\mu(\mathbf{n})]^2, \quad (\text{I.1})$$

where  $C_{11} = C_{22} = Ea/b$  and  $C_{12} = C_{21} = Gb/a$ . Here,  $\hat{1} \equiv \hat{x} \equiv (1, 0)$  and  $\hat{2} \equiv \hat{y} \equiv (0, 1)$ ,  $\delta_{\mu\nu}$  is the Kronecker delta, and the summation extends over all the bonds on the sheet. We note that Poisson's ratio of this system is zero, i.e.,  $G = E/2$  because Eq. (I.1) does not contain the coupling between the displacements in the  $x$ - and  $y$ -directions. Moreover, assuming that the displacements in the  $x$ -direction  $u_1(\mathbf{n})$  for arbitrary  $\mathbf{n}$  are zero at the initial time, forces in the  $x$ -direction are always zero, and thus, every lattice point does not move in the  $x$ -direction. Then, in the following, we consider only the motions and forces in the  $y$ -direction.

To construct the equation of motion for the system, we consider normal and shear forces, together with viscous forces. As illustrated in Fig. S1, the normal and shear forces acting on the lattice point  $\mathbf{n}$  in the  $y$ -direction are given, respectively, as follows:

$$F_{\text{up}} - F_{\text{down}} = Eah \left[ \frac{u_2(\mathbf{n} + \hat{y}) - u_2(\mathbf{n})}{b} - \frac{u_2(\mathbf{n}) - u_2(\mathbf{n} - \hat{y})}{b} \right] = Eabh \frac{\Delta^2}{\Delta y^2} u_2(\mathbf{n}), \quad (\text{I.2})$$

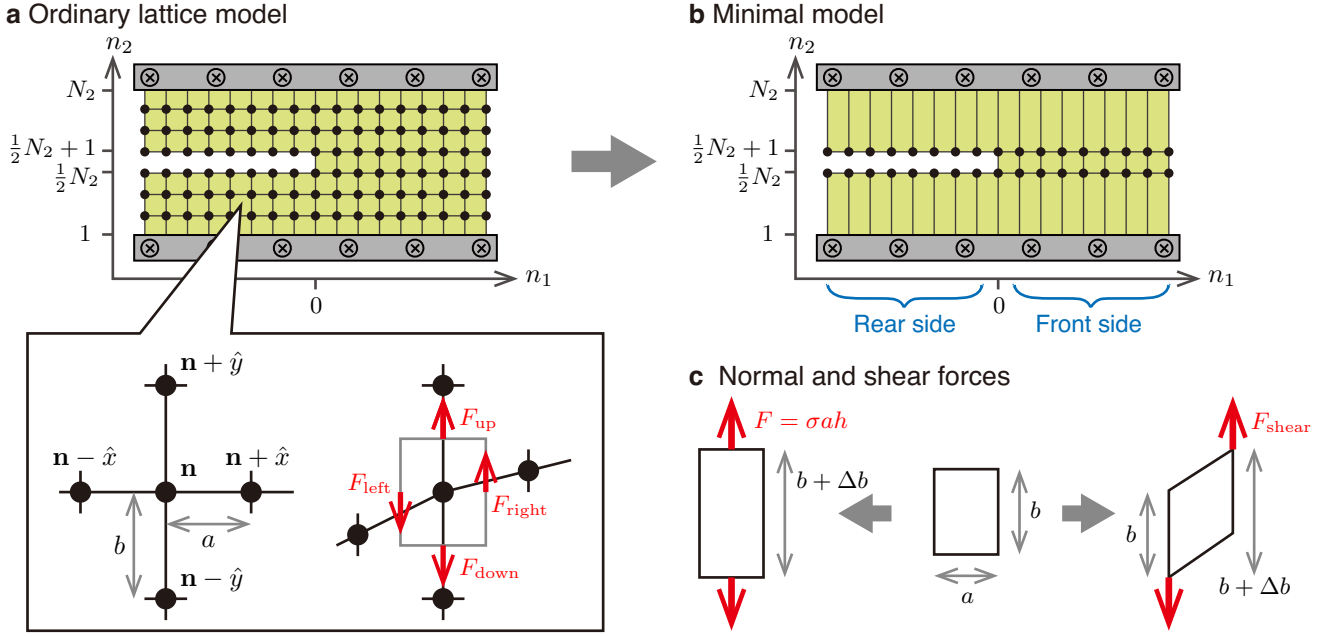


FIG. S1: **Ordinary and minimal lattice models for the fixed-grip crack propagation.** **a**, Lattice model with a rectangular unit cell under zero strain. The lattice point is specified by two integers  $\mathbf{n} = (n_1, n_2)$ . The top and bottom boundaries are located at  $n_2 = 1$  and  $n_2 = N_2$ , respectively, and the two surfaces of the line crack are located at  $n_2 = N_2/2$  and  $n_2 = N_2/2 + 1$ . In the box, magnified views on a lattice point and its nearest neighbor points with and without deformation are shown together with the indices of the points, the lattice constants  $a$  and  $b$ , and associated forces. **b**, Coarse-grained semi-lattice model obtained by removing lattice points except for the ones located at  $n_2 = N_2/2$  and  $n_2 = N_2/2 + 1$ . **c**, Elementary deformation modes of a unit cell in the rectangular lattice with lattice spacings  $a$  and  $b$ .

$$F_{\text{right}} - F_{\text{left}} = Gbh \left[ \frac{u_2(\mathbf{n} + \hat{x}) - u_2(\mathbf{n})}{a} - \frac{u_2(\mathbf{n}) - u_2(\mathbf{n} - \hat{x})}{a} \right] = Gabh \frac{\Delta^2}{\Delta x^2} u_2(\mathbf{n}). \quad (\text{I.3})$$

Here, we have introduced the notations,  $\frac{\Delta^2}{\Delta x^2} f(\mathbf{n}) \equiv [f(\mathbf{n} + \hat{x}) - 2f(\mathbf{n}) + f(\mathbf{n} - \hat{x})]/a^2$  and  $\frac{\Delta^2}{\Delta y^2} f(\mathbf{n}) \equiv [f(\mathbf{n} + \hat{y}) - 2f(\mathbf{n}) + f(\mathbf{n} - \hat{y})]/b^2$ , which correspond to the second-order partial derivatives in the continuum limits,  $a \rightarrow 0$  and  $b \rightarrow 0$ , respectively. When a Kelvin-Voigt element is employed for the interaction in the  $y$ -direction, the following viscous term should be added:

$$F_{\text{up}}^{(\eta)} - F_{\text{down}}^{(\eta)} = \eta ah \left[ \frac{\frac{\partial}{\partial t} u_2(\mathbf{n} + \hat{y}) - \frac{\partial}{\partial t} u_2(\mathbf{n})}{b} - \frac{\frac{\partial}{\partial t} u_2(\mathbf{n}) - \frac{\partial}{\partial t} u_2(\mathbf{n} - \hat{y})}{b} \right] = \eta abh \frac{\Delta^2}{\Delta y^2} \frac{\partial}{\partial t} u_2(\mathbf{n}). \quad (\text{I.4})$$

In this way, the equation of motion of the lattice point  $\mathbf{n}$  in the  $y$ -direction is given by

$$\begin{aligned} m \frac{\partial^2}{\partial t^2} u_2(\mathbf{n}) &= F_{\text{right}} - F_{\text{left}} + F_{\text{up}} - F_{\text{down}} + F_{\text{up}}^{(\eta)} - F_{\text{down}}^{(\eta)} \\ &= abh \left[ G \frac{\Delta^2}{\Delta x^2} u_2(\mathbf{n}) + E \frac{\Delta^2}{\Delta y^2} u_2(\mathbf{n}) + \eta \frac{\Delta^2}{\Delta y^2} \frac{\partial}{\partial t} u_2(\mathbf{n}) \right]. \end{aligned} \quad (\text{I.5})$$

Assuming that we can neglect the inertial term  $m \frac{\partial^2}{\partial t^2} u_2(\mathbf{n})$  (the overdamped limit), we obtain the equation of motion per unit volume in the following form:

$$0 = G \frac{\Delta^2}{\Delta x^2} u_2(\mathbf{n}) + E \frac{\Delta^2}{\Delta y^2} u_2(\mathbf{n}) + \eta \frac{\Delta^2}{\Delta y^2} \frac{\partial}{\partial t} u_2(\mathbf{n}). \quad (\text{I.6})$$

## II. MINIMAL MODEL CONSISTING OF KELVIN-VOIGT ELEMENTS

### A. Construction of a minimal model

In this section, we construct a minimal model for crack propagation in viscoelastic sheets as shown in Fig. S1b, by ignoring all the lattice points except for the lattice points at  $n_2 = N_2/2$  and  $n_2 = N_2/2 + 1$ . The original set of variables  $\{u_2(\mathbf{n})\}$  is now represented by a much smaller set,  $\{u_2(i, N_2/2)\} \cup \{u_2(i, N_2/2 + 1)\}$  for  $i \in \mathbb{Z} \equiv \{\dots, -1, 0, 1, \dots\}$ . For simplicity, we assume that the sheet is always symmetric about the  $x$  axis, and thus the lattice points on the upper side,  $u_i \equiv u_2(i, N_2 + 1)$  for  $i \in \mathbb{Z}$ , completely describe the dynamics of the present model.

In the following discussion, it is important to distinguish three types of strain in the  $y$ -direction (see Fig. S2a; here and hereafter, we set  $l \equiv b$  and use  $l$  instead of  $b$ ):

- (i)  $\varepsilon$ : the global fixed strain;
- (ii)  $\mathcal{E}_i(t)$ : the strain of the  $i$ -th upper (or lower) “long spring,” i.e., the  $i$ -th spring of natural length  $(L - l)/2$  directly connected to the top (or bottom) boundary (the strains of the upper and lower long springs are the same so that we consider only the upper ones and “long springs” indicate the upper ones);
- (iii)  $\mathcal{E}_i^{(l)}(t) \equiv [u_2(i, N_2 + 1) - u_2(i, N_2)]/l = 2u_i/l$ : the strain of the  $i$ -th “short spring,” i.e., the  $i$ -th spring of natural length  $l$  located at the center in the  $y$ -direction (provided that the  $i$ -th short spring exists).

Here,  $\varepsilon$  is a constant, but  $\mathcal{E}_i(t)$  and  $\mathcal{E}_i^{(l)}(t)$  depend on time  $t$ . We mainly use  $\mathcal{E}_i(t)$  to describe the dynamics of crack propagation because  $\mathcal{E}_i^{(l)}(t)$  is expressed by  $\mathcal{E}_i(t)$  by the following relation (see Fig. S2b):

$$L\varepsilon = (L - l)\mathcal{E}_i(t) + l\mathcal{E}_i^{(l)}(t). \quad (\text{II.1})$$

Note that  $\mathcal{E}_i(t)$  is much smaller than  $\mathcal{E}_i^{(l)}(t)$  provided that the  $i$ -th short spring exists because “the spring constant” of long springs is much smaller than that of the short springs (the corresponding Young’s moduli are the same for the short and long springs). To realize crack propagation, we remove the  $i$ -th short spring when  $\mathcal{E}_i^{(l)}(t) \geq \varepsilon_c$ . At places far from the crack tip,  $\mathcal{E}_i(t)$  approaches a constant value and the value depends on whether the  $i$ -th long spring is located on the front (i.e., right) or rear (i.e., left) side of the tip of a crack propagating in the positive  $x$ -direction (see Fig. S1b):

$$\begin{cases} \lim_{i \rightarrow -\infty} \mathcal{E}_i(t) = 0 & \text{rear side} \\ \lim_{i \rightarrow +\infty} \mathcal{E}_i(t) = \lim_{i \rightarrow +\infty} \mathcal{E}_i^{(l)}(t) = \varepsilon. & \text{front side} \end{cases} \quad (\text{II.2})$$

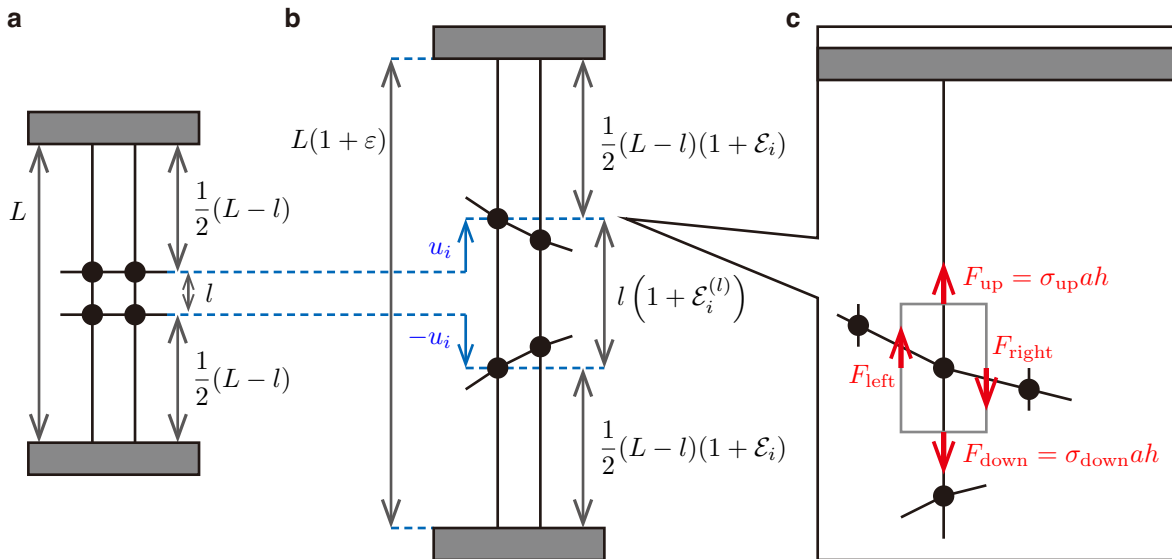


FIG. S2: **Schematic illustration of three types of strain ( $\varepsilon$ ,  $\mathcal{E}_i(t)$ , and  $\mathcal{E}_i^{(l)}(t)$ ) and forces.** **a**, The proposed minimal lattice model under zero strain. We call the springs of length  $(L - l)/2$  and those of length  $l$  the long and short springs, respectively. **b**, The model under the finite strain  $\varepsilon$ . **c**, Forces acting on a lattice point in the model.

We construct the equation of motion in the  $y$ -direction for the  $i$ -th lattice point characterized by  $u_i(t)$  in the minimal model. First, we consider normal stresses on the basis of Eq. (I.6); as illustrated in Fig. S2c, considering the elongational deformation in the  $y$ -direction of the  $i$ -th long and short springs, we obtain the normal stresses acting on the  $i$ -th lattice point in the following form:

$$\begin{cases} \frac{F_{\text{up},i}(t)}{ah} = E_0 \mathcal{E}_i(t) \\ \frac{F_{\text{down},i}(t)}{ah} = E_0 \mathcal{E}_i^{(l)}(t), \end{cases} \quad (\text{II.3})$$

from which, we have  $F_{\text{up},i}(t) - F_{\text{down},i}(t) = E_0 (\mathcal{E}_i(t) - \varepsilon) ahL/l$  by virtue of Eq. (II.1). Here, we display the subscript 0 for the Young's modulus,  $E_0$ , whereas we have omitted the subscript in Sec. I, i.e.,  $E \equiv E_0$ . This is because we should distinguish the two springs  $E_0$  and  $E_1$  in a Zener element, which is a generalization of a Kelvin-Voigt element and will be considered in Secs. III and IV. Second, we consider shear stresses; as illustrated in Fig. S2c, considering the shear deformation in the  $y$ -direction, we obtain  $F_{\text{right},i} - F_{\text{left},i} = ah\mu \frac{\Delta^2}{\Delta x^2} u_i(t)$ . Note that shear modulus  $G$  for the ordinary lattice model (Fig. S1a, discussed in Sec. I) is replaced by the "effective" shear modulus  $\mu$  for the minimal model (Fig. S1b). This is because the shear modulus for the minimal model is considered to effectively represent all the forces acting on the decimated points from the nearest neighbor points located in the  $x$ -directions, with a spirit similar to the one employed in renormalization [S1] in statistical physics. Third, combining the normal and shear stresses together with the viscous terms, we obtain the equations of motion in the  $y$ -direction for the  $i$ -th lattice point of mass  $m$ , by noting that  $F_{\text{down},i}(t)$  and  $F_{\text{down},i}^{(\eta)}(t)$  are missing on the rear side of the crack tip:

$$\begin{cases} m \frac{\partial^2}{\partial t^2} u_i(t) = F_{\text{right},i} - F_{\text{left},i} + F_{\text{up},i} + F_{\text{up},i}^{(\eta)} = ahE_0 \mathcal{E}_i(t) + ah\mu \frac{\Delta^2}{\Delta x^2} u_i(t) & \text{rear side} \\ m \frac{\partial^2}{\partial t^2} u_i(t) = F_{\text{right},i} - F_{\text{left},i} + F_{\text{up},i} - F_{\text{down},i} + F_{\text{up},i}^{(\eta)} - F_{\text{down},i}^{(\eta)} = ah \frac{L}{l} E_0 (\mathcal{E}_i(t) - \varepsilon) + ah\mu \frac{\Delta^2}{\Delta x^2} u_i(t) & \text{front side.} \end{cases} \quad (\text{II.4})$$

Since Eq. (II.1) can be expressed as  $\mathcal{E}_i(t) = [L\varepsilon - 2u_i(t)]/(L - l)$ , we can rewrite the above equations of motion in terms of  $\mathcal{E}_i(t)$  by removing the dynamic variable  $u_i(t)$ . Finally, assuming that the inertial term is negligible (the overdamped limit), we obtain the equations of motion for the field  $\mathcal{E}_i(t)$ :

$$\begin{cases} 0 = E_0 \mathcal{E}_i(t) + \eta \frac{\partial}{\partial t} \mathcal{E}_i(t) - \frac{1}{2} l (L - l) \mu \frac{\Delta^2}{\Delta x^2} \mathcal{E}_i(t) & \text{rear side} \\ 0 = \frac{L}{l} E_0 (\mathcal{E}_i(t) - \varepsilon) + \frac{L}{l} \eta \frac{\partial}{\partial t} \mathcal{E}_i(t) - \frac{1}{2} l (L - l) \mu \frac{\Delta^2}{\Delta x^2} \mathcal{E}_i(t) & \text{front side.} \end{cases} \quad (\text{II.5})$$

We have three comments on the equations of motion (II.5). (i) When shear is neglected ( $\mu = 0$ ), the two expressions in the front and rear sides reduce to the same equation of motion (except for the equilibrium position), which describes the Kelvin-Voigt dynamics. (ii) The "second-derivative" term  $E_0 \frac{\Delta^2}{\Delta x^2} u_2(\mathbf{n})$  in Eq. (I.6) has been replaced by the strain-field term,  $E_0 \mathcal{E}_i(t)$  (rear side) or  $\frac{L}{l} E_0 (\mathcal{E}_i(t) - \varepsilon)$  (front side) in Eq. (II.5) with proportional constants. (iii) The net strains of long springs in the rear and front sides are different and given by  $\mathcal{E}_i(t)$  and  $\mathcal{E}_i(t) - \varepsilon$ , respectively, because  $\lim_{i \rightarrow -\infty} \mathcal{E}_i(t) = 0$  and  $\lim_{i \rightarrow -\infty} \mathcal{E}_i(t) = \varepsilon$  in the rear and front sides, respectively (see Eq. (II.2)).

To derive the equations to be solved analytically, we take the continuum limit of Eq. (II.5) in the  $x$ -direction,  $a \rightarrow 0$ . In this limit, the finite difference  $\frac{\Delta^2}{\Delta x^2}$  is replaced by the derivative  $\frac{\partial^2}{\partial x^2}$  and the discrete strain field  $\mathcal{E}_i(t)$  by the continuum strain field  $\mathcal{E} \equiv \mathcal{E}(\tau, \chi)$  where we have introduced the dimensionless parameters,  $\tau = t/t_0$ ,  $\chi = x/x_0$  with

$$t_0 \equiv \frac{\eta}{E_0} \quad \text{and} \quad x_0 \equiv l \sqrt{\left(1 - \frac{l}{L}\right) \frac{\mu}{2E_0}}. \quad (\text{II.6})$$

In this way, the above discrete version of the equations motion (II.5) is replaced by the following continuum equations:

$$\begin{cases} 0 = \mathcal{E} + \dot{\mathcal{E}} - N \mathcal{E}'' & \text{rear side} \\ 0 = (\mathcal{E} - \varepsilon) + \dot{\mathcal{E}} - \mathcal{E}'' & \text{front side} \end{cases} \quad (\text{II.7})$$

Here, we have introduced the notations,  $\dot{\mathcal{E}} \equiv \frac{\partial}{\partial \tau} \mathcal{E}(\tau, \chi)$ ,  $\mathcal{E}'' \equiv \frac{\partial^2}{\partial \chi^2} \mathcal{E}(\tau, \chi)$ , and

$$N \equiv \frac{L}{l}. \quad (\text{II.8})$$

## B. Derivation of an exact solution of crack propagation with a constant velocity

In this subsection, we solve Eq. (II.7) for the static case ( $V = 0$ ) and for the dynamic case in which a crack propagates with a constant velocity ( $0 < V < \infty$ ), by seeking the solution of the form  $\mathcal{E}(\tau, \chi) = f(\chi - \nu\tau)$ . Here, we have introduced the dimensionless velocity of crack propagation,

$$\nu = \frac{V}{V_0}, \quad (\text{II.9})$$

with  $V_0$  defined by

$$V_0 \equiv \frac{x_0}{t_0} = \frac{l}{\eta} \sqrt{\left(1 - \frac{l}{L}\right) \frac{E_0 \mu}{2}}. \quad (\text{II.10})$$

Substituting  $f(\chi - \nu\tau)$  into Eq. (II.7), we have second-order linear ordinary differential equations:

$$\begin{cases} 0 = f(\chi) - \nu f'(\chi) - N f''(\chi) & \text{for } \chi < 0 \quad (\text{rear side}) \\ 0 = f(\chi) - \varepsilon - \nu f'(\chi) - f''(\chi) & \text{for } 0 \leq \chi \quad (\text{front side}). \end{cases} \quad (\text{II.11})$$

Here, since the width (in the  $x$ -direction) of the sheet is large enough, no generality is lost by setting the position of crack tip to  $\chi = 0$  with  $\tau = 0$ : the crack exists in the region  $\chi < 0$  and is absent in the region  $\chi \geq 0$ .

We give the boundary conditions for the differential equations (II.11) as follows: the conditions at remote edges, (see Eq. (II.2))

$$\begin{cases} f(-\infty) = 0 & \text{rear side} \\ f(+\infty) = \varepsilon & \text{front side} \end{cases} \quad (\text{II.12})$$

and the matching conditions at the crack tip for the strain field  $\mathcal{E}$ ,

$$\begin{cases} f(-0) = f(+0) \equiv f(0) \\ f'(-0) = f'(0). \end{cases} \quad (\text{II.13})$$

As previously mentioned, we remove the short spring (located in the center in the  $y$ -direction with natural length  $l$ , see Fig. S2) when  $\mathcal{E}^{(l)}(t) \geq \varepsilon_c$ . We rewrite this inequality as

$$\mathcal{E}(\tau, \chi) = f(\chi - \nu\tau) \leq f_c \equiv \frac{N\varepsilon - \varepsilon_c}{N - 1}, \quad (\text{II.14})$$

by use of Eq. (II.1). Therefore,  $f(0)$  satisfies (i)  $f(0) > f_c$  for  $\nu = 0$  and (ii)  $f(0) = f_c$  for  $0 < \nu < \infty$ .

We solve the ordinary differential equation (II.11) under the boundary conditions (II.12) and (II.13). First, we solve the differential equation for  $\chi < 0$ . Substituting the form  $f(\chi) = C e^{-\chi/\xi}$  into Eq. (II.11), we obtain the characteristic equation (quadratic equation for  $\xi$ ),

$$g_N(\xi) = \xi^2 + \nu\xi - N = 0, \quad (\text{II.15})$$

and the solutions,

$$\xi_{N,\pm} = \left(-\nu \pm \sqrt{\nu^2 + 4N}\right) / 2. \quad (\text{II.16})$$

From the boundary conditions (II.12) and (II.13), only the solution  $\xi_{N,-}$  is relevant:  $f(\chi) = f(0) \exp(-\chi/|\xi_{N,-}|)$ . Second, we solve the differential equation for  $\chi \geq 0$ . Substituting the form  $f(\chi) - \varepsilon = C e^{-\chi/\xi}$  into Eq. (II.11), we obtain the characteristic equation,  $g_1(\xi) = \xi^2 + \nu\xi - 1 = 0$ , and the solutions,  $\xi_{1,\pm} = \left(-\nu \pm \sqrt{\nu^2 + 4}\right) / 2$ . From the boundary conditions (II.12) and (II.13), only the solution  $\xi_{1,+}$  is relevant:  $f(\chi) = \varepsilon - [\varepsilon - f(0)] \exp(-\chi/\xi_{1,+})$ . Finally, we rewrite the matching condition,  $f'(-0) = f'(0)$  as

$$\frac{f(0)}{|\xi_{N,-}|} = \frac{\varepsilon - f(0)}{\xi_{1,+}}. \quad (\text{II.17})$$

In the following, we determine  $f(\chi)$  from Eq. (II.17) in the cases of  $\nu = 0$  and  $0 < \nu < \infty$ .

In the static case ( $\nu = 0$ ), we can rewrite Eq. (II.17) as  $f(0) = \frac{\sqrt{N}}{\sqrt{N+1}}\varepsilon$ , by using  $|\xi_{N,-}| = \sqrt{N}$  and  $\xi_{1,+} = 1$  from Eq. (II.16). This gives the following solution:

$$\mathcal{E}(\tau, \chi) = f(\chi) = \begin{cases} \frac{\varepsilon\sqrt{N}}{\sqrt{N+1}}e^{\chi/\sqrt{N}} & \text{for } \chi < 0 \quad (\text{rear side}) \\ \varepsilon - \frac{\varepsilon}{\sqrt{N+1}}e^{-\chi} & \text{for } 0 \leq \chi \quad (\text{front side}) \end{cases} \quad (\text{II.18})$$

For  $\nu = 0$ , the inequality  $f(0) > f_c$  yields

$$\tilde{\varepsilon} \equiv \frac{\varepsilon}{\varepsilon_c} < \frac{1}{\sqrt{N}}. \quad (\text{II.19})$$

Note that Eq. (II.19) implies that  $\tilde{\varepsilon} > 1/\sqrt{N}$  in the case of crack propagation,  $\nu > 0$ .

In the case of crack propagation with a constant velocity  $\nu$  ( $0 < \nu < \infty$ ), since  $f(0) = f_c$ , the exact relationship between  $\nu$  and  $\tilde{\varepsilon}$  is obtained from Eq. (II.17) as

$$\nu \equiv \frac{V}{V_0} = \frac{N\tilde{\varepsilon}^2 - 1}{\sqrt{\tilde{\varepsilon}(1-\tilde{\varepsilon})(N\tilde{\varepsilon} - 1)}}, \quad (\text{II.20})$$

or equivalently

$$\tilde{\varepsilon} = \frac{\sqrt{\nu^2 + 4N} + \sqrt{\nu^2 + 4}}{\sqrt{\nu^2 + 4N} + N\sqrt{\nu^2 + 4} - (N-1)\nu}. \quad (\text{II.21})$$

The expression (II.20) does not exhibit the velocity jump in the physically relevant range of  $\tilde{\varepsilon}$ ,  $1/\sqrt{N} < \tilde{\varepsilon} < 1$ . By using Eq. (II.20), we obtain the dynamics of the strain distribution:

$$\mathcal{E}(\tau, \chi) = f(\chi - \nu\tau) = \begin{cases} \frac{N\varepsilon - \varepsilon_c}{N-1} \exp\left[\frac{\chi - \nu\tau}{|\xi_{N,-}|}\right] & \text{for } \chi - \nu\tau < 0 \quad (\text{rear side}) \\ \varepsilon - \frac{\varepsilon_c - \varepsilon}{N-1} \exp\left[-\frac{\chi - \nu\tau}{\xi_{1,+}}\right] & \text{for } 0 \leq \chi - \nu\tau \quad (\text{front side}). \end{cases} \quad (\text{II.22})$$

Here, two healing lengths have been introduced (see Fig. 4e in the main text and Fig. S4c below):

$$|\xi_{N,-}| = \sqrt{\frac{N\tilde{\varepsilon} - 1}{\tilde{\varepsilon}(1-\tilde{\varepsilon})}}, \quad \xi_{1,+} = \sqrt{\frac{1-\tilde{\varepsilon}}{\tilde{\varepsilon}(N\tilde{\varepsilon} - 1)}}. \quad (\text{II.23})$$

Equation (II.20) or (II.21) gives the relation between the velocity  $V$  and the initially applied energy density  $w = \frac{1}{2}E_0\varepsilon^2$ , by virtue of the relation

$$\frac{w}{Nw_0} = \tilde{\varepsilon}^2 \equiv \frac{\varepsilon^2}{\varepsilon_c^2} \quad \text{with} \quad w_0 = \frac{E_0\varepsilon_c^2}{2N}. \quad (\text{II.24})$$

### III. MINIMAL MODEL CONSISTING OF ZENER ELEMENTS 1: THE BASIC EQUATIONS AND EXACT SOLUTION

#### A. Generalization of viscoelastic interaction: equations of motion in the $y$ -direction

In this section, we generalize the present model by changing the interaction from the one based on Kelvin-Voigt elements to the one on Zener elements (see Fig. S3). A Zener element is a parallel connection of the spring  $E_0$  (strain  $\mathcal{E}(t)$ ) and a Maxwell element, which is a serial connection of the spring  $E_1$  (strain  $\mathcal{E}_1(t)$ ) and the dashpot  $\eta$  (strain  $\mathcal{E}_2(t)$ ). The strains of the parallel components are identical:

$$\mathcal{E}(t) = \mathcal{E}_1(t) + \mathcal{E}_2(t). \quad (\text{III.1})$$

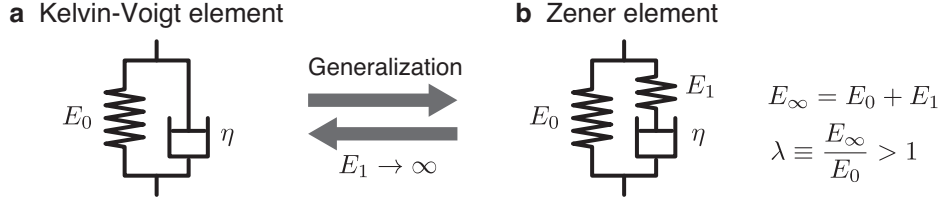


FIG. S3: **Schematic illustrations of (a) Kelvin-Voigt and (b) Zener elements.** We obtain the former as the limit  $E_1 \rightarrow \infty$  from the latter.

For the serial components in the Maxwell element, the stresses on the spring  $E_1$  and dashpot  $\eta$  are identical:

$$\eta \frac{\partial}{\partial t} \mathcal{E}_2(t) = E_1 \mathcal{E}_1(t). \quad (\text{III.2})$$

Note here that a Zener element reduces to a Kelvin-Voigt element in the large  $E_1$  limit (i.e.,  $E_1 \rightarrow \infty$  and  $\mathcal{E}_1(t) = 0$ ) and in the static limit ( $\frac{\partial}{\partial t} \mathcal{E}_2 = 0$ ). The generalization of the equations of motion in the  $y$ -direction is achieved by the following replacements:

$$\begin{cases} \frac{F_{\text{up}}}{ah} + \frac{F_{\text{up}}^{(\eta)}}{ah} = E_0 \mathcal{E} + \eta \frac{\partial}{\partial t} \mathcal{E} & \rightarrow E_0 \mathcal{E} + \eta \frac{\partial}{\partial t} \mathcal{E}_2 \\ \frac{F_{\text{up}}}{ah} + \frac{F_{\text{up}}^{(\eta)}}{ah} - \frac{F_{\text{down}}}{ah} - \frac{F_{\text{down}}^{(\eta)}}{ah} = \frac{L}{l} E_0 \mathcal{E} + \frac{L}{l} \eta \frac{\partial}{\partial t} \mathcal{E} & \rightarrow \frac{L}{l} E_0 \mathcal{E} + \frac{L}{l} \eta \frac{\partial}{\partial t} \mathcal{E}_2. \end{cases} \quad (\text{III.3})$$

With this replacement, Eq. (II.5) in the continuum limit in the  $x$ -direction,  $a \rightarrow 0$ , is given as

$$\begin{cases} 0 = E_0 \mathcal{E} + \eta \frac{\partial}{\partial t} \mathcal{E}_2 - \frac{1}{2} \mu l (L-l) \frac{\partial^2}{\partial x^2} \mathcal{E} & \text{rear side} \\ 0 = \frac{L}{l} E_0 (\mathcal{E} - \varepsilon) + \frac{L}{l} \eta \frac{\partial}{\partial t} \mathcal{E}_2 - \frac{1}{2} \mu l (L-l) \frac{\partial^2}{\partial x^2} \mathcal{E} & \text{front side} \end{cases} \quad (\text{III.4})$$

As in the case of the Kelvin-Voigt interaction, we use the dimensionless parameters,  $\tau = t/t_0$ ,  $\chi = x/x_0$ , and  $N \equiv L/l$ , where  $t_0 \equiv \eta/E_0$ , and  $x_0 \equiv l\sqrt{(L-l)\mu/(2LE_0)}$ . Then, we rewrite the above equations of motion as

$$\begin{cases} 0 = \mathcal{E} + \dot{\mathcal{E}}_2 - N \mathcal{E}'' & \text{rear side} \\ 0 = (\mathcal{E} - \varepsilon) + \dot{\mathcal{E}}_2 - \mathcal{E}'' & \text{front side,} \end{cases} \quad (\text{III.5})$$

where  $\dot{\mathcal{E}}_2 \equiv \frac{\partial}{\partial \tau} \mathcal{E}_2(\tau, \chi)$  and  $\mathcal{E}'' \equiv \frac{\partial^2}{\partial \chi^2} \mathcal{E}(\tau, \chi)$ .

We eliminate  $\mathcal{E}$  in Eq. (III.5) by using the following relation obtained by substituting Eq. (III.2) into Eq. (III.1),

$$\mathcal{E} = \mathcal{E}_2 + \frac{E_0}{E_1} \dot{\mathcal{E}}_2, \quad (\text{III.6})$$

to have the equations of motion for a single field  $\mathcal{E}_2$  in the following form:

$$\begin{cases} 0 = \mathcal{E}_2 + (1+s) \dot{\mathcal{E}}_2 - N \mathcal{E}_2'' - s N \dot{\mathcal{E}}_2'' & \text{rear side} \\ 0 = (\mathcal{E}_2 - \varepsilon) + (1+s) \dot{\mathcal{E}}_2 - \mathcal{E}_2'' - s \dot{\mathcal{E}}_2'' & \text{front side.} \end{cases} \quad (\text{III.7})$$

Here, we have introduced the parameter

$$s \equiv \frac{E_0}{E_1}. \quad (\text{III.8})$$

Equation (III.7) with  $\mathcal{E}_2$  replaced by  $\mathcal{E}$  also holds. This equation for  $\mathcal{E}$  can be obtained either by multiplying the operator  $1 + s \frac{\partial}{\partial \tau}$  to Eq. (III.7) and use  $(1 + s \frac{\partial}{\partial \tau}) \mathcal{E}_2 = \mathcal{E}$  or by eliminating  $\mathcal{E}_2$  in Eq. (III.5).

In the main text, we have used  $\lambda$  defined as

$$\lambda \equiv \frac{E_\infty}{E_0} = 1 + \frac{1}{s}, \quad (\text{III.9})$$

instead of  $s$ . Although the physical meaning of  $\lambda$  is clearer than  $s$ , we mainly use  $s$  in this section for mathematical simplicity. The parameters  $s$  and  $\lambda$  vary in the ranges of  $0 < s < \infty$  and  $1 < \lambda < \infty$ , respectively. Note that the Kelvin-Voigt interaction (finite  $E_0$  and  $E_1 = \infty$ ) corresponds to the limit  $s \rightarrow 0$  or equivalently  $\lambda \rightarrow \infty$ .

### B. Derivation of the exact solution of crack propagation with a constant velocity

In this subsection, we solve Eq. (III.7) in the case of crack propagation with a constant velocity ( $0 < V < \infty$ ). Note that, in the case of  $V = 0$ , a Zener element reduces to a Kelvin-Voigt element, and we have already solved the model consisting of Kelvin-Voigt elements in Sec. II.

We derive the equations of motion with relevant boundary conditions to be solved in the present case, following the manner employed in the Kelvin-Voigt case in Sec. II. We substitute the form  $\mathcal{E}_2(\tau, \chi) = f(\chi - \nu\tau)$  into Eq. (III.7) and derive linear ordinary differential equations for  $f(\chi)$  for  $\chi < 0$  and  $0 \leq \chi$ , where we set the position of the crack tip to  $\chi = 0$  with  $\tau = 0$ . Here,  $V$  and  $\nu = V/V_0$  are the dimensional and dimensionless velocities, respectively, with  $V_0 \equiv x_0/t_0 \simeq lE_0/\eta$  as before (see Eq. (II.10)). We give the result as

$$\begin{cases} 0 = f(\chi) - (1+s)\nu f'(\chi) - Nf''(\chi) + s\nu Nf'''(\chi) & \text{for } \chi < 0 \quad (\text{rear side}) \\ 0 = f(\chi) - \varepsilon - (1+s)\nu f'(\chi) - f''(\chi) + s\nu f'''(\chi) & \text{for } 0 \leq \chi \quad (\text{front side}). \end{cases} \quad (\text{III.10})$$

To determine the boundary conditions, we substitute  $\mathcal{E}_2(\tau, \chi) = f(\chi - \nu\tau)$  into Eq. (III.6) to have  $\mathcal{E} = f - s\nu f'$ . For  $\chi - \nu\tau \rightarrow \pm\infty$ , we have  $\mathcal{E} = f$ , since  $f' = 0$ . For  $\chi - \nu\tau = 0$ , we assume that the strain distributions  $\mathcal{E}$  and  $\mathcal{E}_2$  are continuous and differentiable at the crack tip. The values of the functions and their derivatives match at the crack tip:  $\mathcal{E}(-0) = \mathcal{E}(+0)$ ,  $\mathcal{E}'(-0) = \mathcal{E}'(+0)$ ,  $\mathcal{E}_2(-0) = \mathcal{E}_2(+0)$ , and  $\mathcal{E}'_2(-0) = \mathcal{E}'_2(+0)$  ( $\mathcal{E}'_2(-0) = \mathcal{E}'_2(+0)$  can be derived from the others). In addition, as in the case of the Kelvin-Voigt interaction, we assume that the short spring is absent when  $\mathcal{E}^{(d)} \geq \varepsilon_c$ , which yields  $\mathcal{E}(-0) = \mathcal{E}(+0) = \frac{N\varepsilon - \varepsilon_c}{N-1}$ . In summary, we give the appropriate boundary conditions as

$$\begin{cases} f(-0) - s\nu f'(-0) = f(+0) - s\nu f'(+0) = \frac{N\varepsilon - \varepsilon_c}{N-1}; \\ f'(-0) = f'(+0); & f''(-0) = f''(+0); \\ f(-\infty) = 0; & f(+\infty) = \varepsilon. \end{cases} \quad (\text{III.11})$$

We can then establish the exact analytical relation between the global strain  $\varepsilon$  and the normalized velocity of crack propagation  $\nu \equiv V/V_0$  as in the following theorem:

**Theorem 1. (Relation between global strain and crack-propagation velocity).** *If Eqs. (III.10) and (III.11) hold, then*

$$\tilde{\varepsilon} \equiv \frac{\varepsilon}{\varepsilon_c} = \frac{\nu \left(1 + s + \frac{sN}{\xi_1 \xi_N}\right) + \xi_1 + \xi_N}{\nu \left(1 + sN + \frac{sN}{\xi_1 \xi_N}\right) + N\xi_1 + \xi_N} = \frac{\frac{\nu}{\lambda-1} \left(\frac{N}{\xi_1 \xi_N} + \lambda\right) + \xi_1 + \xi_N}{\frac{\nu}{\lambda-1} \left(N + \frac{N}{\xi_1 \xi_N} + \lambda - 1\right) + N\xi_1 + \xi_N}, \quad (\text{III.12})$$

where

$$\begin{aligned} \xi_N = \frac{1}{6} & \left[ 2^{2/3} \sqrt[3]{3\sqrt{3}\sqrt{-N(4N^2 + N(4(5-2s)s+1)\nu^2 + 4s(s+1)^3\nu^4) + 9N(2s-1)\nu - 2(s+1)^3\nu^3}} \right. \\ & \left. + \frac{2\sqrt[3]{2}(3N + (s+1)^2\nu^2)}{\sqrt[3]{3\sqrt{3}\sqrt{-N(4N^2 + N(4(5-2s)s+1)\nu^2 + 4s(s+1)^3\nu^4) + 9N(2s-1)\nu - 2(s+1)^3\nu^3}} - 2(s+1)\nu \right]. \end{aligned} \quad (\text{III.13})$$

We note that  $\xi_N$  is the positive solution of the cubic equation

$$g_N(\xi) \equiv \xi^3 + (1+s)\nu\xi^2 - N\xi - s\nu N = 0. \quad (\text{III.14})$$

In the limit  $s \rightarrow 0$ ,  $g_N(\xi) = 0$  reduces to the quadratic equation (II.15) appearing in the case of the Kelvin-Voigt interaction. In this limit, Eqs. (III.12) and (III.13) reduce to Eq. (II.21) and  $\xi_N = (\sqrt{\nu^2 + 4N} - \nu)/2$ , respectively. The uniqueness of  $\xi_N$  is ensured by the following lemma.

**Lemma 1.** *Let  $s$ ,  $\nu$ , and  $N$  are positive real numbers. Then,  $g_N(\xi) = 0$  has one positive and two negative real solutions for  $-\infty < \xi < \infty$ .*

We prove Theorem 1 with the aid of Lemma 1 (we give the proof of Lemma 1 at the last of this subsection).

*Proof of Theorem 1.*

First, we solve the differential equation for  $\chi < 0$  (the first equation of Eqs. (III.10)). Substituting the form  $f(\chi) = Ce^{-\chi/\xi}$  into the equation, we obtain the characteristic equation (III.14). According to Lemma 1, we can set the three solutions,  $\xi_{N,1}$ ,  $\xi_{N,2}$ , and  $\xi_N$ , of the cubic equation  $g_N(\xi) = 0$  to satisfy the relation  $\xi_{N,1} < \xi_{N,2} < 0 < \xi_N$ . To satisfy the boundary conditions at  $\xi \rightarrow -\infty$ , the solution of the differential equation for  $\chi < 0$  has the form  $f(\chi) = \sum_{i=1}^2 C_i e^{-\chi/\xi_{N,i}}$ , where  $C_1$  and  $C_2$  will be determined later by using the boundary conditions at  $\chi = 0$ .

Second, we solve the differential equation for  $\chi \geq 0$ . Substituting the form  $f(\chi) - \varepsilon = Ce^{-\chi/\xi}$  into the equation, we obtain the characteristic equation,

$$g_1(\xi) = \xi^3 + (1+s)\nu\xi^2 - \xi - s\nu = 0. \quad (\text{III.15})$$

Note that  $g_1(\xi)$  is identical to  $g_N(\xi)$  with  $N = 1$ . According to Lemma 1,  $g_1(\xi) = 0$  has one positive and two negative real solutions, and we denote the positive solution as  $\xi_1$ . To satisfy the boundary conditions at  $\xi \rightarrow \infty$ , the solution of the differential equation for  $\chi > 0$  has the form  $f(\chi) = \varepsilon - C_0 e^{-\chi/\xi_1}$ , where we can determine  $C_0$  by using the boundary condition at  $\chi = 0$ :

$$\frac{N\varepsilon - \varepsilon_c}{N-1} = f(+0) - s\nu f'(+0) = \varepsilon - C_0 \left(1 + \frac{s\nu}{\xi_1}\right). \quad (\text{III.16})$$

Finally, we determine the relation between  $\tilde{\varepsilon}$  and  $\nu$ , by eliminating  $C_0$ ,  $C_1$ , and  $C_2$  from the boundary conditions,  $f(-0) = f(+0)$ ,  $f'(-0) = f'(+0)$ , and  $f''(-0) = f''(+0)$ , which can be recast into the following forms:

$$\begin{cases} \varepsilon - C_0 = C_1 + C_2 \\ \xi_1^{-1} C_0 = -\xi_{N,1}^{-1} C_1 - \xi_{N,2}^{-1} C_2 \\ -\xi_1^{-2} C_0 = \xi_{N,1}^{-2} C_1 + \xi_{N,2}^{-2} C_2. \end{cases} \quad (\text{III.17})$$

Introducing the parameters  $D_i \equiv C_i/C_0$  and  $\gamma_i \equiv |\xi_1/\xi_{N,i}| = -\xi_1/\xi_{N,i}$ , Eq. (III.17) is written as

$$\begin{cases} D_1 + D_2 = \frac{\varepsilon}{C_0} - 1 = \left(1 + \frac{s\nu}{\xi_1}\right) \frac{N-1}{\tilde{\varepsilon}^{-1} - 1} - 1 \\ \gamma_1 D_1 + \gamma_2 D_2 = 1 \\ \gamma_1^2 D_1 + \gamma_2^2 D_2 = -1. \end{cases} \quad (\text{III.18})$$

From the second and third expressions of Eq. (III.18), we obtain  $D_1 = \frac{\gamma_2 + 1}{\gamma_1(\gamma_2 - \gamma_1)}$  and  $D_2 = \frac{-1 - \gamma_1}{\gamma_2(\gamma_2 - \gamma_1)}$ , which leads

$$D_1 + D_2 = \frac{1}{\gamma_1} + \frac{1}{\gamma_2} + \frac{1}{\gamma_1 \gamma_2}. \quad (\text{III.19})$$

Here, we note that  $\gamma_1 < \gamma_2$ . According to Vieta's Formulae (which is for a polynomial equation and relates the coefficients of the polynomial with sums and products of the roots), the characteristic equation  $g_N(\xi) = 0$  gives  $\xi_{N,1} + \xi_{N,2} + \xi_N = -(1+s)\nu$  and  $\xi_{N,1}\xi_{N,2}\xi_N = s\nu N$ . These two relations are rewritten as

$$\begin{cases} \frac{1}{\gamma_1} + \frac{1}{\gamma_2} = -\frac{\xi_{N,1}}{\xi_1} - \frac{\xi_{N,2}}{\xi_1} = \frac{1}{\xi_1} [(1+s)\nu + \xi_N] \\ \frac{1}{\gamma_1 \gamma_2} = \frac{\xi_{N,1}\xi_{N,2}}{\xi_1^2} = \frac{s\nu N}{\xi_1^2 \xi_N}. \end{cases} \quad (\text{III.20})$$

Substituting Eqs. (III.20) into Eq. (III.19), we have

$$D_1 + D_2 = \frac{1}{\xi_1} [(1+s)\nu + \xi_N] + \frac{s\nu N}{\xi_1^2 \xi_N}. \quad (\text{III.21})$$

TABLE I: The behaviors of  $g_N(\xi)$  as a function of  $\xi$  (left) and  $g_N(\alpha_-)$  as a function of  $N$  (right).

$\xi$	$\alpha_-$			0			$\alpha_+$				
$\frac{\partial}{\partial \xi} g_N(\xi)$	+	0	-	-	-	0	+	$N$			
$g_N(\xi)$	$\nearrow$	$g_N(\alpha_-)$	$\searrow$	$-s\nu N$	$\searrow$	$g_N(\alpha_+)$	$\nearrow$	$s(s-2)\nu^2$			
								$\frac{\partial}{\partial N} g_N(\alpha_-)$	-	0	+
								$g_N(\alpha_-)$	$\searrow$	$s^2\nu^3$	$\nearrow$

Combining this with the first relation in Eq. (III.18), we have Eq. (III.12). Thus, Theorem 1 is proved. (Q.E.D.)

*Proof of Lemma 1.*

We express the equation  $\frac{\partial}{\partial \xi} g_N(\xi) = 0$  as  $3\xi^2 + 2(1+s)\nu\xi - N = 0$  and denote its two solutions as  $\alpha_{\pm} = \left[ -(1+s)\nu \pm \sqrt{\nu^2(1+s)^2 + 3N} \right] / 3$ , where  $\alpha_- < 0 < \alpha_+$ . The behavior of  $g_N(\xi)$  as a function of  $\xi$  is summarized in Tab. I; for  $\alpha_- \leq \xi \leq \alpha_+$ , the function  $g_N(\xi)$  is monotonically decreasing. Then,  $g_N(\alpha_+) < g_N(0) = -s\nu N < 0$ . If  $g_N(\alpha_-) > 0$ ,  $g_N(\xi) = 0$  has one positive and two negative real solutions. Thus, in the following, we show  $g_N(\alpha_-) > 0$ .

To show  $g_N(\alpha_-) > 0$ , we calculate  $g_N(\alpha_-)$  and its derivative as follows:

$$g_N(\alpha_-) = \frac{2}{27} [3N + (s+1)^2\nu^2]^{3/2} + \frac{N\nu}{3} (1-2s) + \frac{2}{27}(s+1)^3\nu^3, \quad (\text{III.22})$$

$$\frac{\partial}{\partial N} g_N(\alpha_-) = \frac{1}{3} [3N + (s+1)^2\nu^2]^{1/2} + \frac{\nu}{3} (1-2s), \quad (\text{III.23})$$

$$\frac{\partial^2}{\partial N^2} g_N(\alpha_-) = \frac{1}{2} [3N + (s+1)^2\nu^2]^{-1/2}. \quad (\text{III.24})$$

Since  $s$ ,  $\nu$ , and  $N$  are positive real numbers,  $\frac{\partial^2}{\partial N^2} g_N(\alpha_-) > 0$ , which means that  $\frac{\partial}{\partial N} g_N(\alpha_-)$  is a monotonically increasing function. Now,  $\frac{\partial}{\partial N} g_N(\alpha_-) = 0$  at  $N = s(s-2)\nu^2$ , at which  $g_N(\alpha_-)$  takes the minimum value as a function of  $N$ . Since  $g_N(\alpha_-)|_{N=s(s-2)\nu^2} = s^2\nu^3$  is positive,  $g_N(\alpha_-) > 0$  for any  $N$ . Thus, Lemma 1 is proved. (Q.E.D.)

#### IV. MINIMAL MODEL CONSISTING OF ZENER ELEMENTS 2: LOW- AND HIGH-VELOCITY REGIMES AND VELOCITY JUMP

In this section, we use Eq. (III.12) to investigate the dependences of the initially applied energy density  $w$  on the velocity  $\nu \equiv V/V_0$  in low- and high-velocity regimes, and derive the existence condition of the velocity jump. Note that Eq. (III.12) gives the relation between the initially applied global strain  $\varepsilon$  and  $\nu$  and that  $\varepsilon$  is related to  $w$  simply as  $w = \tilde{\varepsilon}^2 N w_0$  (see Eq. (II.24)). In the following, the present model will be analyzed for arbitrary positive real number  $s \equiv E_0/E_1 > 0$ , which is equivalent to  $\lambda \equiv E_{\infty}/E_0 = 1 + 1/s > 1$ . Note that the relations derived below are further simplified for rubbers, because of the relation  $1 \ll \lambda \ll N$  (typically  $\lambda \simeq 10^2$ – $10^3$  and  $N \simeq 10^6$ – $10^9$ ).

##### A. Low- and high-velocity regimes

To obtain the asymptotic forms of the initially applied energy  $w$  in the low- and high-velocity regimes, we evaluate that of the characteristic equation (III.14). We rewrite this equation as

$$\frac{g_N(\xi)}{N^{3/2}} = \Xi^3 + \frac{\lambda v}{\lambda - 1} \Xi^2 - \Xi - \frac{v}{\lambda - 1} = 0, \quad (\text{IV.1})$$

where  $\Xi \equiv \xi/\sqrt{N}$  and  $v \equiv \nu/\sqrt{N}$ . We denote the positive real solution of Eq. (IV.1) as  $\Xi_+ \equiv \xi_N/\sqrt{N}$ , where  $\xi_N$  is the positive real solution of Eq. (III.14). We note that  $\Xi_+$  is independent of  $N$  and depends only on  $v$  ( $0 < v < \infty$ ) and  $s$ , as seen from Eq. (IV.1). Then, we give the relation between  $\xi_N$  and  $\xi_1$  as  $\Xi_+(v) = \xi_N(\nu/\sqrt{N})/\sqrt{N} = \xi_1(\nu)$ . By evaluating the asymptotic forms of  $\Xi_+$  in the low- and high-velocity regimes, we have the following lemma:

**Lemma 2.** *If  $0 < v \equiv \nu/\sqrt{N} < \infty$  and  $1 < \lambda < \infty$ , then the positive real solution  $\xi_N$  of the characteristic*

equation (III.14),  $g_N(\xi) = 0$ , has the following asymptotic forms:

$$\frac{1}{\sqrt{N}} \xi_N(\nu) \equiv \Xi_+(\nu) = \begin{cases} 1 - \frac{\nu}{2} + O(\nu^2) & (\nu \rightarrow 0) \\ \frac{1}{\sqrt{\lambda}} + \frac{(\lambda-1)^2}{2\nu\lambda^2} + O\left(\frac{1}{\nu^2}\right) & (\nu \rightarrow \infty). \end{cases} \quad (\text{IV.2})$$

Note here that (i) if  $\nu \equiv V/V_0 \ll \sqrt{N}$ , then  $\xi_N(\nu) \simeq \sqrt{N}$ ; and (ii) if  $\nu \gg \sqrt{N}(\lambda-1)^2/\lambda^{3/2}$ , then  $\xi_N(\nu) \simeq \sqrt{N/\lambda}$ .

*Proof of Lemma 2.*

We evaluate the asymptomatic form of  $\Xi_+$  in the vicinity of  $\nu = 0$  (i.e., in the low-velocity regime). Because of the asymptotic behavior,  $g_N(\xi)/N^{3/2} \xrightarrow{\nu \rightarrow 0} \Xi^3 - \Xi$ , We can express Eq. (IV.1) as  $\Xi^3 - \Xi = 0$ , which gives the positive real solution,  $\Xi = 1$ . To evaluate the next order, we introduce the perturbation parameter  $\epsilon_0$ . Substituting  $\Xi = 1 + \epsilon_0$  into Eq. (IV.1), we have

$$2\epsilon_0 + \nu + O(\epsilon_0^2, \epsilon_0\nu) = 0, \quad (\text{IV.3})$$

whose solution is  $\epsilon_0 = -\nu/2 + O(\nu^2)$ . Therefore, we have the expression,  $\Xi_+ = 1 - \nu/2 + O(\nu^2)$ .

Similarly, we evaluate the asymptomatic form of  $\Xi_+$  in the vicinity of  $1/\nu = 0$  (i.e., in the high-velocity regime,  $\nu \gg 1$ ). Because of the asymptotic behavior,  $g_N(\xi) \cdot (\lambda-1)/(vN^{3/2}) \xrightarrow{\nu \rightarrow \infty} \lambda\Xi^2 - 1$ , Eq. (IV.1) can be expressed as  $\lambda\Xi^2 - 1 = 0$ , which gives the positive real solution,  $\Xi = 1/\sqrt{\lambda}$ . Introducing the perturbation parameter  $\epsilon_\infty$ , and substituting  $\Xi = 1/\sqrt{\lambda} + \epsilon_\infty$  into Eq. (IV.1), we have

$$\frac{2\sqrt{\lambda}}{\lambda-1} \nu \epsilon_\infty - \frac{\lambda-1}{\lambda^{3/2}} - \frac{\lambda-3}{\lambda} \epsilon_\infty + \frac{\lambda}{\lambda-1} \nu \epsilon_\infty^2 + \frac{3}{\sqrt{\lambda}} \epsilon_\infty^2 + \epsilon_\infty^3 = 0. \quad (\text{IV.4})$$

Since  $1 < \lambda < \infty$ ,  $|\epsilon_\infty| \ll 1$ , and  $\nu^{-1} \ll 1$ , the first and second terms on the left-hand side of Eq. (IV.4) are the leading-order terms. Thus, the solution of Eq. (IV.4) is  $\epsilon_\infty = \frac{1}{2\nu} \left(\frac{\lambda-1}{\lambda}\right)^2 + O(\nu^{-2})$ . Therefore, we have the expression,  $\Xi_+ = \frac{1}{\sqrt{\lambda}} + \frac{1}{2\nu} \left(\frac{\lambda-1}{\lambda}\right)^2 + O(\nu^{-2})$ . (Q.E.D)

From Theorem 1, with the aid of Lemma 2, we can evaluate  $\tilde{\varepsilon}(\nu)$  in the vicinity of  $\nu = 0$  and that of  $\nu = \infty$ . In the vicinity of  $\nu = 0$ ,  $\xi_N(\nu) = \sqrt{N} - \frac{\nu}{2} + O(\nu^2)$  and  $\xi_1(\nu) = 1 - \frac{\nu}{2} + O(\nu^2)$ . Then, together with Eq. (III.12), we can evaluate  $\tilde{\varepsilon}(\nu)$ . Similarly, in the vicinity of  $\nu = \infty$ ,  $\xi_N(\nu) = \sqrt{\frac{N}{\lambda}} + \frac{N(\lambda-1)^2}{2\nu\lambda^2} + O\left(\frac{1}{\nu^2}\right)$  and  $\xi_1(\nu) = \frac{1}{\sqrt{\lambda}} + \frac{(\lambda-1)^2}{2\nu\lambda^2} + O\left(\frac{1}{\nu^2}\right)$ . Then, together with Eq. (III.12) we can evaluate  $\tilde{\varepsilon}(\nu)$ . We summarize the evaluation in the following theorem.

**Theorem 2 (Asymptotic forms in low- and high-velocity regimes).** *If  $\lambda > 1$  and  $N > 1$ , then*

$$\tilde{\varepsilon}(\nu) = \frac{1}{\sqrt{N}} + \frac{\sqrt{N}-1}{2N} \nu + O(\nu^2) \quad (\nu \rightarrow 0) \quad (\text{IV.5})$$

and

$$\tilde{\varepsilon}(\nu) = \frac{\lambda}{\sqrt{N} + \lambda - 1} - \frac{(\lambda-1)^2 (\sqrt{N}-1) (\sqrt{N}+2)}{2\nu\sqrt{\lambda} (\sqrt{N} + \lambda - 1)^2} + O\left(\frac{1}{\nu^2}\right) \quad (\nu \rightarrow \infty). \quad (\text{IV.6})$$

Equation (IV.5) enables us to evaluate the relation between the initially applied energy density  $w$  and the crack-propagation velocity  $V$  in the low-velocity regime (by virtue of the relation  $w = \tilde{\varepsilon}^2 N w_0$ , see Eq. (II.24)). From Eq. (IV.5), we have  $\lim_{\nu \rightarrow 0} \tilde{\varepsilon}(\nu) = 1/\sqrt{N}$ , or equivalently

$$\lim_{\nu \rightarrow 0} w(\nu) = w_0. \quad (\text{IV.7})$$

Comparing the first and second terms on the right-hand side of Eq. (IV.5), we can estimate the range of  $\nu$  in which  $w(\nu) \simeq w_0$  holds: if  $1/\sqrt{N} \gg \nu(\sqrt{N}-1)/N$ , i.e.,

$$\nu \equiv \frac{V}{V_0} \ll \frac{\sqrt{N}}{\sqrt{N}-1} \quad (\text{IV.8})$$

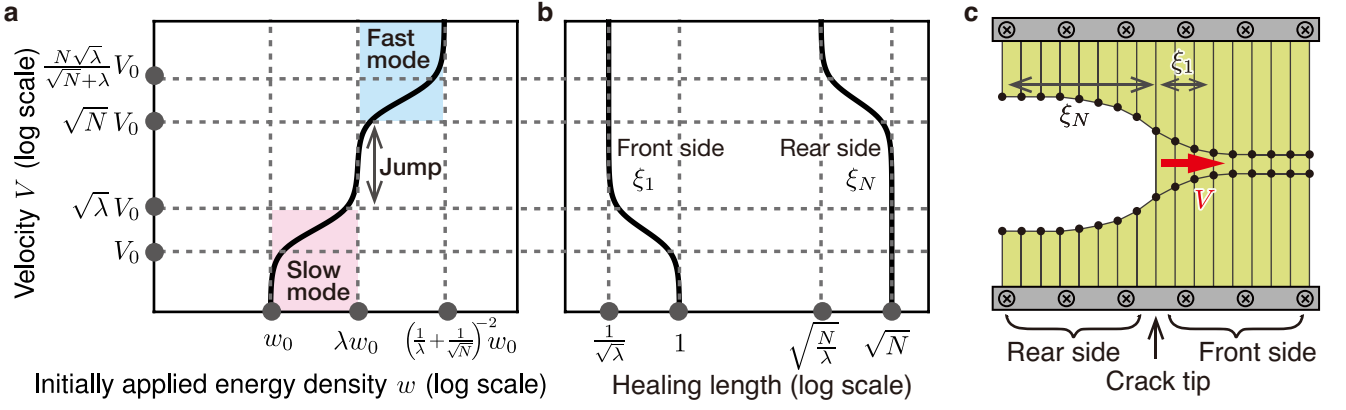


FIG. S4: **Representative plots for typical rubbers** ( $\lambda = 10^3$ ,  $N = 10^9$ ). **a**,  $w$  vs.  $V$ ; the velocity jump appears because the condition  $\lambda \ll N$  is satisfied. **b**,  $\xi_1$  and  $\xi_N$  as a function of  $V$ . **c**, Graphical definitions of the healing length.  $\xi_1$  and  $\xi_N$  correspond to the healing length in the front and rear sides, respectively, that is, distances over which the disturbance of the stress and strain distributions (mainly in the front side) and the crack shape (in the rear side) recover to the remote values (see Eq. (II.21)); as seen in (b), these healing lengths play the roles of order parameters in the context of conventional phase transitions such as superconductors and Bose-Einstein condensations [S2].

is satisfied, then  $w(\nu) \simeq w_0$  (Here, we have omitted the factor 2 in the second term on the right-hand side of Eq. (IV.5)). When  $\sqrt{N} \gg 1$ , the condition (IV.8) is simplified as

$$V \ll V_0. \quad (\text{IV.9})$$

Similarly, Eq. (IV.6) enables us to evaluate the  $w$ - $V$  relation in the high-velocity regime. From the first term on the right-hand side of Eq. (IV.6), we have  $\lim_{\nu \rightarrow \infty} \tilde{\varepsilon}(\nu) = \lambda/(\sqrt{N} + \lambda - 1)$ , or equivalently

$$\lim_{\nu \rightarrow \infty} w(\nu) = \frac{\lambda^2 N w_0}{(\sqrt{N} + \lambda - 1)^2}. \quad (\text{IV.10})$$

We can estimate the range of  $\nu$  in which  $w(\nu) \simeq \lambda^2 N w_0 / (\sqrt{N} + \lambda - 1)^2$  holds, following the manner we employed in the low-velocity case. However, we should pay attention to the fact that Eq. (IV.6) is insufficient for the estimation in the case of (unrealistic) large  $\lambda$ . In fact, for example, in the Kelvin-Voigt limit ( $\lambda \rightarrow \infty$ ) the second term on the right-hand side of Eq. (IV.6) goes to zero. Thus, in this discussion, we assume  $\lambda \lesssim N$ , which includes the case of typical viscoelastic materials ( $1 \ll \lambda \ll N$ ). Comparing the first and second terms on the right-hand side of Eq. (IV.6), we have the range of  $\nu$  in which  $w(\nu) \simeq \lambda^2 N w_0 / (\sqrt{N} + \lambda - 1)^2$  holds: if the crack propagation velocity is sufficiently high, i.e.,

$$\nu \gg \frac{(\sqrt{N} + 2)(\sqrt{N} - 1)(\lambda - 1)^2}{(\sqrt{N} + \lambda - 1)\lambda^{3/2}} \quad (\text{IV.11})$$

is satisfied, then  $w(\nu) \simeq \lambda^2 N w_0 / (\sqrt{N} + \lambda - 1)^2$ . In the case of  $\sqrt{N} \gg 1$  and  $\lambda \gg 1$ , which includes the case of typical viscoelastic materials, the above statement can be simplified, i.e., if

$$\nu \gg \frac{\lambda^{1/2} N}{\sqrt{N} + \lambda} \quad (\text{IV.12})$$

is satisfied, then  $\tilde{\varepsilon}(\nu) \simeq \frac{\lambda}{\sqrt{N} + \lambda}$ , or equivalently

$$w(\nu) \simeq \left( \frac{1}{\sqrt{N}} + \frac{1}{\lambda} \right)^{-2} w_0. \quad (\text{IV.13})$$

We summarize characteristic scales derived from Lemma 2 and Theorem 2 for  $1 \ll \lambda \ll N$  in Fig. S4, together with the scales associated with the jump derived in the next subsection.

### B. Existence condition of the velocity jump

From Theorem 1, with the aid of Lemma 2, we can derive the existence condition of the velocity jump as in the following theorem.

**Theorem 3 (Existence condition of the velocity jump.)** *If  $1 < \lambda < \infty$  and*

$$\frac{\lambda - 1}{\sqrt{\lambda}} \ll \sqrt{N}, \quad (\text{IV.14})$$

*then the approximate expression*

$$\tilde{\varepsilon}(\nu) \equiv \frac{\varepsilon(\nu)}{\varepsilon_c} \simeq \sqrt{\frac{\lambda}{N}} \quad (\text{IV.15})$$

*is valid in the range of  $\nu$ ,*

$$\frac{\lambda - 1}{\sqrt{\lambda}} \ll \nu \ll \sqrt{N}. \quad (\text{IV.16})$$

*Proof of Theorem 3.*

We evaluate the positive solution of the characteristic equation (III.14) under the condition (IV.16). According to Lemma 2, the positive solution of the characteristic equation  $g_N(\xi) = 0$  is expressed as  $\xi \simeq \xi_N^{(0)} \equiv \sqrt{N}$  for  $\nu \ll \sqrt{N}$ . Similarly, the positive solution of  $g_1(\xi) = 0$  is expressed as  $\xi \simeq \xi_1^{(\infty)} \equiv 1/\sqrt{\lambda}$  for  $(\lambda - 1)^2/\lambda^{3/2} < (\lambda - 1)/\lambda^{1/2} \ll \nu$ . Then, Eq. (III.12) can be expressed as

$$\tilde{\varepsilon} \equiv \frac{\varepsilon}{\varepsilon_c} \simeq \frac{\frac{\nu}{\lambda-1} \left( \frac{N}{\xi_1^{(\infty)} \xi_N^{(0)}} + \lambda \right) + \xi_1^{(\infty)} + \xi_N^{(0)}}{\frac{\nu N}{\lambda-1} \left( 1 + \frac{1}{\xi_1^{(\infty)} \xi_N^{(0)}} \right) + \nu + N \xi_1^{(\infty)} + \xi_N^{(0)}} = \frac{\frac{\nu}{\lambda-1} (\lambda + \sqrt{\lambda N}) + \frac{1}{\sqrt{\lambda}} + \sqrt{N}}{\frac{\nu}{\lambda-1} (N + \sqrt{\lambda N}) + \nu + \frac{N}{\sqrt{\lambda}} + \sqrt{N}}. \quad (\text{IV.17})$$

By noting the relation,  $\frac{1}{\sqrt{\lambda}} + \sqrt{N} < \sqrt{\lambda} + \sqrt{N} \ll \frac{\nu}{\lambda-1} (\lambda + \sqrt{\lambda N})$ , for the numerator in Eq. (IV.17), and the relation,

$$\frac{N}{\sqrt{\lambda}} + \sqrt{N} \ll \frac{\nu N}{\lambda-1} \left( 1 + \sqrt{\frac{\lambda}{N}} \right), \quad (\text{IV.18})$$

for the denominator in Eq. (IV.17), we obtain

$$\tilde{\varepsilon} \simeq \frac{\sqrt{\lambda N} + \lambda}{N + \sqrt{\lambda N} + \lambda - 1} \simeq \frac{\sqrt{\lambda N} + \lambda}{N + \sqrt{\lambda N}} = \sqrt{\frac{\lambda}{N}}. \quad (\text{IV.19})$$

(Q.E.D.)

We have two remarks for Theorem 3: (i) the present model consisting of Kelvin-Voigt elements (which corresponds to  $\lambda \rightarrow \infty$ ) never satisfies the existence condition of velocity jump in Eq. (IV.14) because  $N$  is finite; (ii) if  $\lambda \gg 1$ , then the existence condition (IV.14) reduces to

$$\sqrt{\lambda} \ll \sqrt{N}. \quad (\text{IV.20})$$

---

[S1] Cardy, J. *Scaling and renormalization in statistical physics* (Cambridge Univ. press, Cambridge, 1996).

[S2] Leggett, A. J. *Quantum Liquids: Bose condensation and Cooper pairing in condensed-matter systems* (Oxford Univ. Press, Oxford, 2006).